

1 Seasonal and spatial pattern of bio- and photodegradation
2 in boreal humic waters

3
4 Artem V. Chupakov¹, Natalia V. Neverova¹, Anna A. Chupakova¹, Svetlana A. Zabelina¹,
5 Liudmila S. Shirokova^{1,2}, Taissia Ya. Vorobyeva¹, Oleg S. Pokrovsky^{2,3*}

6
7 ¹ Institute of Ecological Problems of the North, N. Laverov Federal Center for Integrated Arctic
8 Research, Nab Severnoi Dviny 23, Arkhangelsk 163000, Russia

9 ² Geoscience and Environment Toulouse, UMR 5563 CNRS, University of Toulouse, 14 Avenue
10 Edouard Belin, Toulouse 31400, France

11 ³ BIO-GEO-CLIM Laboratory, Tomsk State University, 35 Lenina Pr., Tomsk 634050, Russia

12
13 *corresponding author email: oleg.pokrovsky@get.omp.eu

14 Key words: bog, lake, stream, organic matter, metal, bacteria, sunlight

15
16 Synopsis:

17
18 In boreal (non-permafrost) humic (>15 mg DOC/L) waters of a stratified lake and an
19 ombrotrophic bog, the experimentally measured rate of DOM photodegradation is 4 times higher
20 than that of biodegradation. However, given the shallow (0.5 m) photic layer versus the full depth
21 of water column (2 - 10 m), the biodegradation may provide the largest contribution to aerial
22 CO₂ emission.

23
24
25 Submitted to *Biogeosciences*, after revision June 2024

33 **Abstract**

34 Studying competitive effects of microbial and light-induced degradation of dissolved
35 organic matter (DOM) is crucially important for understanding the factors controlling aquatic
36 carbon (C) transformation in boreal waters. However, studies addressing both DOM and trace
37 element (TE) behavior are limited, which does not allow assessment of coupled C – TE
38 (including macro- and micronutrients and toxicants) biogeochemical cycles in these
39 environmentally important settings. Here we characterized the degree of DOM and related major
40 and TE transformation under biotic activity and sunlight using conventional incubations of humic
41 surface waters from the European subarctic: an ombrotrophic peatbog continuum (subsurface
42 water - peatland pool - stream) and a stratified forest lake across seasons.

43 Along the bog water continuum in July, biodegradation rate was the highest in subsurface
44 waters and the lowest in the acidic peatland pool (0.17 to 0.03 mg C L⁻¹ d⁻¹, respectively).
45 Photodegradation was similar for subsurface waters and the stream (about 0.3 mg C L⁻¹ d⁻¹), but
46 was not detectable in the peatland pool. The waters of forest lake exhibited a strong seasonal
47 effect of biodegradation, which was the highest in October and the lowest in June (0.04 and 0.02
48 mg C L⁻¹ d⁻¹, respectively). The photodegradation of DOM from the forest lake was observed
49 only in June and August (0.19 and 0.07 mg C L⁻¹ d⁻¹, respectively). Biodegradation was capable
50 of removing between 1 and 7 % of initial DOC, being the highest in the forest lake in October
51 and in peatland pool in summer. The photolysis was capable of degrading a much higher
52 proportion of the initial DOC (10-25 %), especially in the forest lake during June and the bog
53 stream during July. The change of optical parameters confirmed the highest photodegradation
54 occurs in June (Arctic summer) and demonstrates a decrease of chromophoric (aromatic)
55 compounds during incubation, whereas biodegradation acted preferentially on aliphatic, low
56 molecular weight compounds. Only a few trace metals were sizably affected by both photo- and
57 biodegradation of DOM (Fe, Al, Ti, Nb and light REE), whereas V, Mn, Co, Cu and Ba were

68 affected solely by biodegradation. Typical values of TE removal over a 2-week period of
69 incubation ranged from 1 to 10 %. These effects were mostly pronounced in the less acidic forest
60 lake compared to the bog waters. A likely mechanism of TE removal was their coprecipitation
61 with coagulating Fe(III) hydroxides after destabilization of DOM-Fe complexes.

62 When averaged across sites and seasons, DOM biodegradation and photodegradation
63 processes could remove 5.3 and 10.8 mg C L⁻¹ y⁻¹, respectively. Compared to typical CO₂
64 emissions from inland waters of the region, biodegradation of DOM can provide the totality of
65 C-CO₂ evasion from lake water surfaces whereas bio- and photodegradation are not sufficient to
66 explain the observed fluxes in bog water continuum. Overall, these results demonstrated strong
67 spatial and seasonal variability in DOM and TE complexes bio- and photodegradation, which
68 was poorly accessed until now, and call for the need of a systematic assessment of both processes
69 across seasons with high spatial resolution.

70

71 **1. Introduction**

72 Organic Carbon (OC) processing via metabolic biological (heterotrophic bacteria uptake
73 and respiration) and inorganic physico-chemical (photolysis) pathways is considered to be one
74 of the major source of CO₂ supersaturation in surface waters and related C emissions (Lapierre
75 et al., 2013; Tranvik et al., 2009), although the relative role of dissolved vs particulate organic
76 carbon (POC) remains poorly quantified (e.g. Attermeyer et al., 2018; Lau et al., 2021; Shirokova
77 et al., 2021; Raudina et al., 2022). Recently, in a thorough study of permafrost-affected river,
78 Keskitalo et al. (2022) demonstrated much faster degradation of autochthonous POC during
79 summer compared to that of allochthonous POC during freshet and underlined the importance
80 of considering the interaction between dissolved and particulate phases for characterising fluvial
81 carbon dynamics. Given sizable C emissions in boreal and subarctic waters (Karlsson et al.,
82 2021), together with high concentrations of DOC (Cole et al., 2007; Vonk et al., 2015), and fast

83 ongoing and predicted environmental changes in high latitude aquatic and terrestrial ecosystems
84 (Wauthy et al., 2018; Chaudhary et al., 2020; Harris et al., 2022), the surface waters of subarctic
85 regions are at the forefront of studies on the biogeochemical cycle of C. Although emissions from
86 these waters are significantly lower than those in the 10 °S – 10 °N equatorial belt (e.g., Borges
87 et al., 2015), the magnitude of possible changes in C flux from northern waters to the atmosphere
88 remains much less known. Further, there are still important geographical biases linked to
89 insufficient knowledge of rates and mechanisms of DOC transformation in certain regions. An
90 example is wetland-dominated northern aquatic settings, where high concentrations of soil
91 organic C surrounding the bogs provide elevated concentrations of DOC. These soils and their
92 organic C content become highly vulnerable to biological and physico-chemical impact
93 depending on local environmental context, permafrost presence and season (Vonk et al., 2015).

94 Thorough laboratory and field work on DOM bio- and photolability conducted over the
95 past decades have demonstrated both phenomena are important, and, depending on
96 environmental setting (nutrient regime, photic layer depth, nature of DOM, etc.), one or another
97 may dominate overall DOM removal in surface waters (Vachon et al., 2016, 2017; Vähätalo and
98 Wetzel, 2008; Obernosterer and Benner, 2004). Recently, specific attention was devoted to the
99 aquatic systems of permafrost peatlands given their high vulnerability to climate warming and
100 huge potential for release of soil organic C to surface waters (Vonk et al., 2015; Shirokova et
101 al., 2019; Payandi-Rolland et al., 2020; Prijac et al., 2022; Rosset et al., 2022; Taillardet et al.,
102 2022). These studies provided a range of DOM susceptibility to biotic degradation. Thus,
103 between 10 and 40 % of the DOC in lakes, rivers and soil waters of the boreal zone may be
104 available for bacterial uptake over a time frame of several weeks (Berggren et al., 2010; Roehm
105 et al., 2009). This range is consistent with 14-16% of biodegradable DOC (BDOC) assessed
106 globally (Begum et al. 2022). The necessity for further studies was also indicated, most notably
107 with regard to *i*) seasonal aspects, given that the overwhelming majority of available studies were

108 performed during Arctic summer (see discussions in Vonk et al., 2015; Laurion et al., 2021), and
109 *ii*) increased spatial resolution, given that sizable variations of BDOC can be observed within
110 quite short distances of a hydrological continuum (Payandi-Rolland et al., 2020; Raudina et al.,
111 2022). Another poorly studied aspect is DOM photo- and biolability across the depth of the water
112 column, especially in seasonally stratified lakes which are subject to spring and autumn overturn.

113 Based on a compilation of available studies on BDOC and their own research, Vonk et
114 al. (2015) argued there is a negligible amount of biodegradable DOC in aquatic systems without
115 permafrost. This is, however, contradictory to available assessments on biodegradation of aquatic
116 DOM as major driver of CO₂ emission in general (Amaral et al., 2021; Liu and Wang, 2022) and
117 in boreal waters in particular (Ask et al., 2012; Lapierre et al., 2013). Furthermore, among all
118 Arctic rivers, the highest annual (20%) and winter (ca. 45%) biodegradable DOC (BDOC) was
119 reported for the Ob River, which drains through peatlands with minimal permafrost influence
120 (Wickland et al., 2012). These non-exhaustive examples illustrate certain inconsistency in
121 current estimations of DOC biodegradability in surface organic-rich waters of high latitudes,
122 which precludes quantitative modeling of future C fluxes between land, water and atmosphere in
123 these environmentally important regions. Towards addressing these inconsistencies, in this study,
124 we chose a typical hydrological continuum in a boreal ombrotrophic bog in a glacial lake-ridge
125 complex that includes subsurface water, a small peatland pool in the central part of the bog and
126 an outlet stream. Further, we selected a well-studied deep stratified humic lake in the same region
127 (Lake Temnoe; Chupakov et al., 2017) where we sampled surface and deep horizons for the
128 incubation experiments. The chosen waters represent subarctic non-permafrost regions that
129 exhibit sizable organic C pool in their soils and high concentrations of DOC in their surface
130 waters. In contrast to previous studies of permafrost peatlands (Shirokova et al., 2019; Laurion
131 et al., 2021; Payandi-Rolland et al., 2020; Mazoyer et al., 2022) where the main source of DOM
132 is peat or ground vegetation like mosses and lichens, in this highly productive southern taiga

133 region, DOC may be more vulnerable to microbial activity due to the presence of forest leachates
134 (i.e., Don and Kalbitz, 2005; Kalbitz et al., 2003; Kawahigashi et al., 2004; Kiikkilä et al., 2013)
135 and much higher bioproductivity for both the terrestrial and aquatic parts of the lake-river
136 ecosystems.

137 The first working hypothesis behind our study design is that the DOC-rich subsurface
138 water and deep horizons of the humic lake are mostly sensitive to sunlight impact (Stubbins et
139 al., 2010), and that maximal impact of photodegradation is expected during allochthonous
140 aromatic DOM input (high surface inflow to lakes and bogs in June and October). In contrast,
141 maximal biodegradation of DOM is expected during periods of possible phytoplankton bloom in
142 August, when autochthonous organic material is generated in the water column. An important
143 novelty of the present study is addressing trace metal (TM) partitioning during bio- and
144 photodegradation. The link between DOM and TE is straightforward: in humic waters of
145 peatlands, most TE (except probably some alkalis and oxyanions) are strongly (> 80%)
146 associated to DOM in the form of organic and organo-mineral (Fe, Al) colloids (Pokrovsky et
147 al., 2005, 2012, 2016). As a result, any DOM transformation processes may directly control the
148 pattern of TE. From the other hand, some TE may be photosensitive (Mn, Fe), toxic (Al, Cu, As,
149 Cd, Pb), or limiting micronutrients (Zn, Co, Ni, Mo) for the bacteria. Our second working
150 hypothesis here is that removal of DOM via photo- or bio-degradation will change the
151 partitioning of trace elements which are 1) strongly bound to DOM, such as divalent transition
152 metals, or 2) incorporated into organo-mineral (Fe, Al) colloids, such as trivalent and tetravalent
153 hydrolyses. The TE of 1st group might either remain in solution (during photodegradation),
154 hence not modifying their total dissolved concentration, or being taken up by growing bacteria
155 during bio-degradation of TE-bound organic matter (Shirokova et al., 2017a, c). The elements of
156 the second group are capable of co-precipitating with Fe and Al hydroxides hence being
157 scavenged from the aqueous solution.(e.g., Kopacek et al., 2005, 2006). To test these

158 hypotheses, we examined DOM and related trace metals bio- and photodegradability aiming to
159 assess 1) spatial variations along a hydrological continuum of non-permafrost peatland and
160 different horizons of a neighboring deep stratified lake located in the forest, and 2) temporal
161 variability during 3 main hydrological seasons (high flow in June, baseflow in August and
162 autumn rain season in October) in the forest lake. Achieving these objectives should allow
163 quantifying the relative share of bio- and photodegradation on overall DOC and TM removal
164 from surface waters via biotic and physico-chemical mechanisms.

165

166 **2. Materials and Methods**

167 *2.1. Natural settings of subarctic bog and stratified lake*

168 The study site is in the NE part of the European boreal zone (Arkhangelsk region), **Fig.**
169 **1**. The mean annual air temperature is 0 °C and average annual precipitation is 700 ± 50 mm.
170 The pristine ombrotrophic Ilasskoe Bog is located 30 km SE of Arkhangelsk, and is a typical
171 lake-ridge complex formed from the last glaciation approximately 10,000 years ago. Its total
172 surface area is 89 km², with an average peat thickness of 3 m. The hydrological continuum of the
173 Ilasskoe Bog includes subsurface water collected via piezometer (2-2.5 m depth), a small lake
174 (Severnoe) and a stream outlet (**Fig. 1**). Lake Severnoe, located in the central part of the bog, is
175 a typical peatland pool with an average depth of 1.5 m and a surface area of 0.013 km². The
176 Chernyi Stream is an outlet for the eastern part of the bog. The stream is 0.7-2.0 m wide, 10 km
177 long and it flows in a forested (taiga) zone in the shade of tree canopy. The waters of the Ilasskoe
178 Bog are acidic (pH ranges from 3.9-4.0 in piezometer and peatland pool to 5.7 in stream Chernyi),
179 organic-rich (DOC is equal to 88, 13 and 38 mg L⁻¹ in the piezometer, lake and stream,
180 accordingly) and low mineralized (Electrical Conductivity is 17-46 μS cm⁻¹), as listed in **Table**
181 **1**.

182 Lake Temnoe is located in a pristine forest 100 km NNE of the town of Arkhangelsk, an
183 area that does not receive any direct anthropogenic impact (**Fig. 1**). The watershed area is 3.08
184 km² and the lake surface area is 0.091 km², with a maximum depth of 37 m and a Secchi disk
185 depth of 3.5±0.5 m. The water residence time in the lake is 394 days. Bogs constitute 31% of
186 lake's watershed area, which is represented by carbonate-free loamy moraine atop the peat,
187 podzol and gley soils. The lake water is slightly acidic (pH = 5.1 to 6.0), humic (DOC = 13-20
188 mg L⁻¹) and dominated by allochthonous DOM with a low concentration of total dissolved ions
189 (Electrical Conductivity of 20 µS cm⁻¹). Similar to other deep boreal and subarctic lakes, the lake
190 exhibits 2 main periods of pronounced stratification (November to April and June to September)
191 and two periods of lake overturn (October and May). Maximal winter stratification occurs in
192 March; the highest water temperature typically occurs in July (see Chupakov et al., 2017 for
193 details).

194 The surface waters were collected from the shore (peatland pool and stream) or a PVC
195 boat (Lake Temnoe). Surface (30-50 cm depth) waters were sampled in the Ilaskoe bog and 3
196 water horizons (0.5, 5 and 10 m) were sampled in the Temnoe Lake using a pre-cleaned
197 polycarbonate horizontal water sampler (Aquatic Research Co, ID, USA). The water samples
198 were placed into 2-L Milli-Q pre-cleaned PVC jars and kept refrigerated (4 °C) until arrival at
199 the laboratory within 2-3 hours of collection.

200

201 *2.2. Experiments*

202 2.2.1. Biodegradation

203 For biodegradation assessments we followed the recommended protocol and used the
204 appropriate type of labware for assessing biodegradable DOC of Arctic waters without external
205 nutrient addition (Vonk et al., 2015; Payandi-Rolland et al., 2020) and applied a slight
206 modification from Shirokova et al. (2019) to assess maximal possible biodegradation. Initial

207 water samples brought to the laboratory within 2-3 hours after sampling were filtered through 3
208 μm sterilized Nylon Sartorius membranes (47 mm diameter); these were used because
209 'conventional' 0.8-1.2 μm (GF/F) filtration membranes might remove too many microbial cells
210 (Dean et al., 2018).

211 Duplicate 30 mL aliquots of 3 μm -filtered water were placed into pre-combusted (4.5
212 hours at 450°C) dark borosilicate 40 mL glass bottles wrapped in Al foil to prevent any
213 photolysis, without nutrient amendment and incubated at $22\pm 1^\circ\text{C}$ in the dark. The bottles were
214 closed with loosened sterilized PVC caps. The bottles were shaken manually once a day avoiding
215 the liquid touching the cap. The entire reactor was used for sampling after 0, 2, 5, 8, 12, and 21
216 days of exposure. Sampled solutions were filtered through sterile, MilliQ-cleaned Sartorius 0.22
217 μm filters. The DOC blanks for these filters did not exceed 1% of DOC concentrations in
218 experimental samples. Sterilized control reactors were filled with natural water that was filtered
219 through a 0.22 μm sterile filter and incubated together with experimental reactors following the
220 approach of Köhler et al (2002).

221 All handling and sampling of bottles was performed in the laminar hood box in a sterilized
222 workspace. Filtered samples were acidified with 30 μL of concentrated (8.1 M) double distilled
223 HCl, tightly capped and stored in the refrigerator before DOC analyses. The non-acidified portion
224 of filtrate was used for pH, Specific Conductivity, DIC and $\text{UV}_{254\text{ nm}}$ and optical spectra
225 measurement. Control runs were 0.22 μm sterile-filtered water which was incubated in parallel
226 with experiments and re-filtered through 0.22 μm filters the day of sampling. To ensure
227 minimized release from sterilized Nylon membrane, we ran blank (Milli-Q) filtrations through
228 both GF/F and 0.22 μm Nylon filters; in both cases the DOC blank was below 0.1-0.2 mg/L
229 which is less than 1% of DOC concentration in our samples. The glass bottles were incubated in
230 duplicates at $22\pm 1^\circ\text{C}$ and agitated manually at least once a day over the 16 days of exposure.

231

232 2.2.2. Photodegradation

233 For photodegradation incubations, water samples were collected in Al-foil covered pre-
234 cleaned polypropylene jars and sterile filtered (0.22 μm Nalgene Rapid-Flow Sterile Systems)
235 within 2 hours of sampling and refrigerated. The filtrates were transferred under laminar hood
236 box into sterilized, acid-washed quartz tubes (150 mL volume, 20% air headspace) with silicate
237 stoppers and placed at 3 ± 2 cm depth into an outdoor pool which was filled by river water having
238 the light transparency similar to that of the Ilaskoe and Temnoe lakes. The outdoor pools were
239 placed in an unshaded area with a latitude similar to the sampling sites (< 30 km from Ilaskoe
240 Bog and Temnoe Lake). Slight wind movement and regular manual shaking allowed for
241 sufficient mixing of reactor interiors during exposure. All photodegradation experiments were
242 run in duplicates. The water temperature (EBRO EBI 20) and light intensity (Luxmeter Testo
243 545) were continuously recorded every 3 hours.

244 For photodegradation experiments, we followed conventional methods requiring
245 exposure of 0.2 μm -sterile filtered samples in quartz reactors in the outdoor pool (Vähätalo et al.,
246 2003; Chupakova et al., 2018; Gareis and Lesack, 2018), solar simulator (Lou and Xie, 2006;
247 Amado et al., 2014) or directly in the lake water (Laurion and Mladenov, 2013; Groeneveld et
248 al., 2016). Note that the 0.22 μm sterile filtration is the only way of conducting photodegradation
249 experiments, given that autoclave sterilization of DOM-rich natural waters would coagulate
250 humic material and thereby would not be suitable (Andersson et al., 2018). Filtration through a
251 smaller pore size, however, would decrease the concentration of DOC and trace metals (i.e., Ilina
252 et al., 2014; Vasyukova et al., 2010). We have chosen a 16 day exposure time for logistical
253 constraints, which is still consistent with biodegradation experiments described above and with
254 the duration used in previous studies on photodegradation under sunlight, from 15 to 70 days
255 (Moran et al., 2000; Vähätalo and Wetzel, 2004; Mostofa et al., 2007; Chupakova et al., 2018).
256 Dark control experiments were conducted also in duplicates, using sterilized glass tubes filled

257 with sterile 0.22 μm -filtered water, wrapped in Al foil and placed in the same outdoor pool as
258 the experiments. The headspace (approx. 20% of total reaction volume) was similar in
259 experimental and control reactors. The individual reactors were sterile sampled at the beginning
260 and after the 0, 2, 5, 8, 12, and 16 days of exposure. Each sampling sacrificed the entire reactor.
261 The Milli-Q blanks were collected and processed to monitor for any potential sample
262 contamination introduced by our filtration, incubation, handling and sampling procedures. The
263 organic carbon blanks of the filtrates did not exceed 0.2 mg/L.

264

265 *2.3. Analyses*

266 The temperature, pH, O₂ and specific conductivity in surface waters were measured in
267 the field. The dissolved CO₂ concentration in the studied bodies of water was measured in-situ
268 using submersible Vaissala Carbocap® GM70 handheld carbon dioxide meter with GMP222
269 probes (accuracy 1.5%; see Serikova et al. (2018, 2019) for methodological details). The
270 diffusional CO₂ flux was calculated using a wind-based model (Cole and Caraco, 1998) with k_{600}
271 $= 2.07 + 0.215 \times u_{10}^{1.7}$, where u_{10} is the wind speed at 10 m height, following the approaches
272 developed for surface waters of peatlands (Zabelina et al., 2021).

273 The DOC and DIC were analyzed by high-temperature catalytic oxidation using a
274 Shimadzu® TOC-VCSN (uncertainty $\pm 2\%$, 0.1 mg L⁻¹ detection limit). DIC was measured after
275 sample acidification with HCl and DOC was analyzed in acidified samples after sparging it with
276 C-free air for 3 min at 100 mL min⁻¹ as non-purgable organic carbon (NPOC). Internationally
277 certified water samples (MISSISSIPPI-03 and Pérade-20) were used to check validity and
278 reproducibility of the analysis. Filtered samples collected from photodegradation experiments
279 were acidified with ultrapure nitric acid and analyzed for major and TE following the procedures
280 employed by GET (Geoscience and Environment Toulouse) for analyses of boreal humic waters
281 (Oleinikova et al., 2017, 2018).

282 The UV- and visual absorbance of water samples was measured using a 10 mm quartz
283 cuvette on a CARY-50 UV-vis spectrophotometer to assess the aromaticity of pore fluids via
284 specific UV absorbance (SUVA₂₅₄). In the filtrates, we measured optical density at 254 nm and
285 at selected wavelengths (365, 436, 470, and 665 nm) as well as the entire UV-visible spectrum.
286 The specific UV-absorbency (SUVA₂₅₄, L mg⁻¹ m⁻¹) and E₄₇₀:E₆₆₅ ratios are used as a proxy for
287 degree of condensation of aromatic groups of DOM, or humification (Chin et al., 1994; Weishaar
288 et al., 2003; Hur et al., 2006; Peacock et al., 2013). The ratio E₂₅₄:E₄₃₆ is useful for evaluation
289 of contributions of autochthonous (aquatic) DOM compared to terrestrial (soil) C (Hur et al., 2006;
290 Ilina et al., 2014). The ratio E₂₅₄:E₃₆₅ also allows approximating the mean molecular weight of
291 DOM (Hiriart-Baer et al., 2008; Berggren et al., 2007). For better visualization of the differences
292 in spectral parameters between experimental and control reactors, we calculated the difference
293 (ΔA) between the absorbance of the photo- or bio-reactor and that of the control reactor at each
294 sampling time.

295 Major cations, Si, P and ~40 TE were measured with a quadrupole ICP-MS (Agilent 7500
296 ce) using In and Re as internal standards. The international geo-standard SLRS-6 (Riverine Water
297 Reference Material for Trace Metals) was used to check validity and reproducibility of analyses.
298 Note that for both bio- and photodegradation experiments, ICP MS analyses were performed
299 over 16 days of incubation time.

300 To check for possible microbial development in biodegradation experiments, we
301 performed oligotrophic and eutrophic bacteria counts over the course of incubation, following
302 the standard methodology used in biodegradation experiments of peat waters (Stutter et al., 2013)
303 and also described previously (Shirokova et al., 2017b; Chupakova et al., 2018). Specifically,
304 active bacteria number count (colony forming units, CFU mL⁻¹) was performed using Petri dishes
305 inoculation (0.1 to 1.0 mL of lake water in three replicates) performed in a laminar hood box
306 immediately prior the experimental incubation start and upon each sampling. Samples were

307 inoculated on Nutrient Agar (5 g L⁻¹ beef extract, 5 g L⁻¹ gelatine peptone, 15 g L⁻¹ bacteriological
308 agar, pH=6.8±0.2 at 25 °C) to determine the total number of heterotrophic bacteria. Difco® agar
309 (granulated powder, Lot No 6290083) inoculation was used to assess the number of oligotrophic
310 bacteria. Inoculation of blanks was routinely performed to assure the absence of contamination
311 from external environments.

312

313 2.4. Data treatment

314 The bio- and photodegradable DOC and trace metals were calculated as percent loss
315 relative to control in similar fashion with other studies (Vonk et al., 2015; Chupakova et al.,
316 2018; Shirokova et al., 2017b, 2019). However, previous works in similar environmental contexts
317 of high-DOC humic waters demonstrated that the effects of DOC and element decrease are rather
318 low and often comparable to uncertainties of duplicates (Shirokova et al., 2019). To assess the
319 net effect of bio- or photodestruction during the experiment, we used the integral values of
320 concentration change, estimated as the difference between the experiment and the control, while
321 taking into account the standard deviation of replicates. For this, we first calculated the mean of
322 replicates at the *i*-th time of sampling for the experiment and the control of *X* component ($^{mean}X_i$
323 and $^{control}X_i$, respectively). We next calculated the sum of mean concentration of replicates and
324 its standard deviation ($^{mean}X_i+SD_i$). Thus, we obtained 3 values characterizing the bio- or photo-
325 degradation process: 1) the change of concentration in the experimental reactor (^{mean}S), 2) the
326 change of concentration not linked to the studied process ($^{control}S$), and 3) the maximal uncertainty
327 of the concentration change in the reactor ($^{mean+SD}S$). This allowed calculating, in percentages,
328 the efficiency of bio or photodegradation of *X* component relative to the control, taken into
329 account relevant uncertainties as following:

$$330 \quad X (\%) = 100 \times (|^{mean}X| - |^{control}X|) / |^{control}X| \quad (1)$$

$$331 \quad SD (\%) = 100 \times (|^{mean+SD}X| - |^{mean}X|) / |^{control}X| \quad (2)$$

332 where X is biodegradable DOC or trace element (BDOC and BTE, respectively) or
333 photodegradable DOC and trace element (PDOC and PTE, respectively). The sign of X
334 designates either a decrease («-») or an increase («+») of solute concentration during the
335 experiment. We considered the decrease of concentration significant when X (%) > SD (%). In
336 other cases, the change was non-systematic over the course of experiment or non-measurable
337 using the experimental technique employed in the present study.

338 The mean rate of bio- or photodegradation of X component (V_X) was calculated based on
339 the overall change (ΔX , in %) between the initial (X_0) and final value normalized to overall
340 duration of the experiment t (22 and 16 days for bio- and photodegradation, respectively):

$$341 \quad V_X = ((\Delta X/X_0) / t \quad (3)$$

342 The SD for rates of component change were calculated in a similar way.

343 The spectral differences between experimental and control reactors were presented as X-
344 Y-Z diagrams where X is elapsed time, Y is wavelength, and Z is ΔA . The data were plotted in
345 a Surfer software package using triangulation with a linear interpolation method. Statistical
346 treatment included the least squares method and the Pearson correlation, as the data were
347 normally distributed. All calculations were performed in STATISTICA ver. 10 (StatSoft
348 Inc.,Tulsa) at $p = 0.05$).

349

350 **3. Results**

351 *3.1. Field measured C concentration and calculated CO₂ fluxes*

352 The DOC concentration ([DOC]) ranged from 13 to 21 mg L⁻¹ in Lake Temnoe,
353 depending on depth and season. The CO₂ concentrations and fluxes increased from June to
354 October and varied from 99 to 220 μmol L⁻¹ and 32 to 71 mmol CO₂ m⁻² d⁻¹, respectively (**Table**
355 **1**). In Ilasskoe Bog hydrological continuum, the DOC decreased from 88 mg L⁻¹ in the peat soil
356 water to 38 mg L⁻¹ in the outlet stream. The DOC concentration was generally similar (within ±

357 5 %) between 3, 0.8 (GFF), 0.45 and 0.22 μm pore size filtration of the initial sample, which is
358 in agreement with former size fractionation measurements for Arctic and subarctic systems
359 (Vasyukova et al., 2010; Pokrovsky et al., 2012, 2016, Shirokova et al., 2019). The waters of
360 Ilaskoe Bog continuum exhibited CO_2 supersaturation with respect to atmosphere (from 55 to
361 3300 $\mu\text{mol L}^{-1}$) and calculated CO_2 emission (diffusion) flux ranging from 22 $\text{mmol CO}_2 \text{ m}^{-2} \text{ d}^{-1}$
362 in the peatland pool to 1600 $\text{mmol CO}_2 \text{ m}^{-2} \text{ d}^{-1}$ in the piezometer (**Table 1**).

363

364 *3.2. DOC concentration evolution in the experiments*

365 3.2.1. Biodegradation

366 In the Temnoe Lake, the range of [DOC] change during 2-3 week incubation in the
367 experimental reactors did not exceed 2 mg L^{-1} and remained within +0.5 to -1.5 mg L^{-1} , which is
368 less than 10% of the initial DOC amount (**Fig. 2 and Fig. S1** of the Supplement). The
369 biodegradable DOC was both season and depth dependent and ranged from 2 to 6 % (**Table 2**).
370 The integral 2-week rates of biodegradation (**Table 3, Fig. 3 A**) demonstrated the highest values
371 during autumn at depths of 0.5 m and 10 m and the lowest values during June at all depths. The
372 final 0-10 m water column- and season-averaged biodegradation rate in Lake Temnoe ranged
373 from 0.02 to 0.04 $\text{mg DOC L}^{-1} \text{ d}^{-1}$. Integral rates of bio-degradation in the 0-10 m layer
374 demonstrated an increase from May to October, over the entire open-water period (**Fig. 4**).

375 For Ilaskoe Bog, the BDOC was highest in the peatland pool (4.9 ± 1.4 %) and lowest
376 in the outlet stream (3.1 ± 2.4 %; **Fig. 2 and Fig. S1**). The integral rate of DOC biodegradation
377 followed the order 'piezometer >> stream > peatland pool' and ranged from 0.03 to 0.17 mg C
378 $\text{L}^{-1} \text{ d}^{-1}$ (**Table 3, Fig. 3 A**).

379

380

381

382 3.2.2. Photodegradation

383 Compared to biodegradation, photodegradation demonstrated much higher values of
384 PDOC and rates of reaction as well as higher variability among seasons and sites. In Lake
385 Temnoe, the PDOC was the highest in June and the lowest in October (**Fig. 2 B** and **Table 2**).
386 The maximal range of concentration change during 2-week period achieved 6-8 mg L⁻¹ (**Fig. S2**)
387 which was 10 to 20 % of the initial [DOC] values. The rates strongly decreased from May-June
388 to the end of summer – autumn. The depth integrated (0 to 10 m) rate of DOM photodegradation
389 in Lake Temnoe ranged from 0 in October to 0.2 mg C L⁻¹ d⁻¹ in June (**Table 3; Fig. 4 B**).

390 In the Ilasskoe Bog hydrological continuum during July, the photodegradation rate
391 followed the order “outlet stream > piezometer >> peatland pool” (**Fig. 3 B**), where integral rates
392 equaled to 0.27±0.04, 0.33±0.07, and 0±0.05 mg C L⁻¹ d⁻¹, respectively (**Table 3**).

393

394 *3.3. Optical parameters of DOM*

395 3.3.1 Biodegradation

396 In Lake Temnoe, the SUVA₂₅₄ remained relatively constant (4.2 to 4.6 L mg C⁻¹ m⁻¹)
397 across seasons and depths (**Table 1 B**). Over the course of biodegradation, the SUVA₂₅₄ did not
398 change significantly (i.e., less than 0.2 units, which is comparable to the variability of duplicates;
399 **Fig. S3**). The ratio E₂₅₄:E₄₃₆, which is an indicator of humification, increased with incubation
400 time in Lake Temnoe waters; the magnitude of this increase across depth followed the order “0.5
401 m > 5 m > 10 m” (**Fig. S4**). The ratio E₂₅₄/E₃₆₅ also increased over the course of biodegradation,
402 corresponding to an increase of mean molecular weight of DOM (Hiriart-Baer et al., 2008;
403 Berggren et al., 2007). The ratio E₃₆₅/E₄₇₀ also demonstrated the strongest increase in surface
404 horizons and virtually no change in the deepest horizon (**Fig. S4**). An increase in the ratio
405 E₄₇₀:E₆₆₅ corresponds to a decrease in the degree of aromaticity (humification). An increase in
406 the ratio E₂₅₄:E₄₃₆ signifies a decrease in contribution of autochthonous (aquatic) DOM compared

407 to terrestrial (soil) C, whereas an increase in the $E_{254}:E_{365}$ ratio characterizes removal of low
408 molecular weights compounds.

409 In Ilasskoe Bog samples, the highest SUVA was observed in the water of the piezometer
410 and the lowest in the stream, but the evolution of this parameter in the course of biodegradation
411 was rather weak (**Fig. S4**). The $E_{254}:E_{365}$ and $E_{254}:E_{436}$ ratios increased with incubation time in
412 the piezometer and decreased with time in the stream (**Fig. S4**). The optical ratios ($E_{254}:E_{436}$,
413 $E_{365}:E_{470}$, $E_{470}:E_{665}$) increased in the peatland pool, suggesting an increase in the molecular
414 weight and an increase in the ratio of aromatic to aliphatic compounds.

415 Complete spectral differences between the experimental and control samples
416 demonstrated rather weak ($\Delta A \leq 0.04$) changes of spectral parameters, mostly detectable after
417 10-12 days of incubation (**Fig. S5**). These results were generally consistent with the discrete
418 spectral parameters presented above and demonstrated maximal effects in the piezometer and
419 bog outlet stream. In Lake Temnoe, the maximal impact of biodegradation on spectral parameters
420 was observed in June, at 0.5 m depth.

421

422 3.3.2. Photodegradation

423 Similar to the DOC concentration, the optical parameters of DOM more strongly evolved
424 over the course of photodegradation compared to the biodegradation experiments. In the Temnoe
425 Lake, the strongest decrease in $SUVA_{254}$ was observed in the waters of all horizons in June. This
426 decrease was less pronounced in October (**Fig. S6**). The $E_{254}:E_{365}$ ratio demonstrated a sizable
427 increase in June, with much weaker increase in October. The $E_{254}:E_{436}$ ratio strongly decreased
428 with exposure time throughout all seasons (10 m depth) and only in June in the surface horizons
429 (**Fig. S7**). An increase in the ratio $E_{254}:E_{365}$ over the course of photodegradation corresponded to
430 an increase in mean molecular weight of DOM. The ratios $E_{365}:E_{470}$ and $E_{470}:E_{665}$ decreased in

431 all experiments with the Temnoe Lake waters (**Fig. S7**), suggesting a decrease in the degree of
432 humification (Battin, 1998) and a decrease in the ratio of aromatic to aliphatic moieties.

433 The SUVA₂₅₄ in Ilasskoe Bog waters remained stable during photodegradation of stream
434 waters and piezometer and strongly decreased in the peatland pool (**Fig. S6**). The E₂₅₄:E₄₃₆ ratio
435 strongly increased in the peatland pool and exhibited a decrease in stream waters and piezometer,
436 whereas the E₃₆₅:E₄₇₀ ratio systematically decreased in all photodegradation experiments with the
437 Ilasskoe Bog continuum (**Fig. S7**). Finally, the E₄₇₀:E₆₆₅ ratio exhibited sizable decrease, in the
438 order 'stream >> pool ≥ piezometer'. The total spectral differences between experimental and
439 control reactors were mostly pronounced in stratified forest lake waters in June ($\Delta A = -0.4$ to -
440 0.4) and in the bog continuum in July, where effects were strongest in the piezometer and outlet
441 stream waters (ΔA parameter as high as - 0.4 (**Fig. S8**)).

442

443 *3.4. Bacterial number evolution during biodegradation experiments*

444 The number of cultivable eutrophic bacteria (EB) sizably (ca., 2 orders of magnitude)
445 increased during biodegradation of Lake Temnoe waters. However, this evolution was not
446 systematic in the course of incubation; there was a pronounced decrease after 2 weeks of
447 exposure in June and August and rather stable concentration in waters of all horizons sampled in
448 October (**Fig. S9**). Such maxima in June and August might be linked to consumption of
449 substrate/nutrient limitations on bacterial growth. In Ilasskoe Bog continuum, the number of
450 eutrophic bacteria decreased by an order of magnitude in the peatland pool and piezometer while
451 it remained constant in the stream. The number of oligotrophic bacteria (OB) increased in waters
452 of all Lake Temnoe horizons by ca. 2 orders of magnitude in August and October and 1 order of
453 magnitude in June. In contrast, the OB number did not change or slightly decreased during
454 incubations of waters from Ilasskoe Bog continuum (**Fig. S9**).

455

456 3.5. Trace element patterns

457 3.5.1 TE in biodegradation experiments

458 During biodegradation experiments, a number of trace metals [Group 1] demonstrated a
459 significant ($X > SD$, Eqn. 1) decrease in concentration across the incubation period (**Table 2**):
460 Al, Ti, Fe, Co, Cu, Ba, Nb, light REE (LREE) and Pb (as illustrated for Fe in **Fig. 5**) as well as
461 Mn, V, and La (**Figs. S10, S11 and S12**, respectively). The most significant effects were
462 observed for Fe in the 0-5 m horizon of Lake Temnoe (9 to 18 % in June, 6 to 13.5 % in August
463 and 8 to 9.5 % in October) and 14% in the peatland pool of Ilasskoe Bog. Overall, for most
464 elements except Fe and Mn, this increase was less pronounced than that of DOC; maximal effects
465 were achieved for Lake Temnoe in August and October (V, Mn, Co, Cu, Ni, Nb, Hf, Pb and Th)
466 and in June (Al and Ti). These elements are typically linked to DOM and Fe and present in the
467 form of organic- and organo-mineral colloids. Second group of major and trace elements did
468 not appreciably change their concentration ($< 2\%$ decrease): Li, B, Na, Mg, K, Ca, Si, Ge, As,
469 Rb, Sr, Mo, Sb, Mo and Ba. These elements are not linked to colloids of Fe(III) hydroxide and
470 organic matter. Finally, some elements [Group 3] exhibited unstable behavior without systematic
471 change in concentration during the exposure ($X < SD$, Eqns. 1-2): Cr, Zn, Cu, Sr, Cd, (Y, Zr),
472 Cs, Tl and U. These elements cannot be considered as significantly impacted by the
473 biodegradation process in Lake Temnoe water.

474 In the Ilasskoe Bog hydrological continuum, the most significant changes during
475 biodegradation were observed in the peatland pool and outlet stream. Elements strongly ($> 5-10$
476 %; $X > S.D.$ in Eqn. 1) affected by biodegradation were V, Fe, Ni, Ga, Y, LREEs and Pb.

477

478 3.5.2. TE in photodegradation experiments

479 The elements affected by photodegradation also formed three groups similar to those
480 impacted by biodegradation. Concentrations of Al, Fe, trivalent and tetravalent hydrolysates (Ti,

481 Ga, Zr, Y, LREE and Th) and Nb of [Group 1] significantly ($> 2\%$; $p < 0.05$) decreased during
482 photolysis as illustrated for Fe in **Fig. 6**, and for Ti and Zr in **Figs. S13** and **S14**, respectively.
483 The decrease of Fe was mostly pronounced in Lake Temnoe water from 10 m depth, whereas
484 that of Ti and Zr was detectable for all horizons and seasons except in October. For the Ilasskoe
485 Bog continuum, there was no systematic change in Fe concentration, whereas concentrations of
486 Ti and Zr systematically decreased over the course of sunlight exposure (**Figs. S13, S14**). Alkali
487 (Li, Rb), alkaline-earth metals (Mg, Ca, Sr, Ba), Si and oxyanions (As, Mo, Sb) of [Group 2]
488 were weakly ($< 2\%$) affected by photolysis. Finally, the remaining trace elements of [Group 3]
489 did not exhibit any systematic evolution of concentration during exposure to sunlight, or these
490 changes were inferior to the uncertainties of replicates ($X < S.D.$ in Eqn. 1).

491 We found that, unlike for DOC, the magnitude of trace element concentration decrease
492 during photodegradation was generally lower than that of biodegradation experiments. Overall,
493 the strongest effects were observed for Ti (3 to 9% in Lake Temnoe; 20% in Ilasskoe Bog), Ga
494 (6 to 14%), Zr (14-17% in Lake Temnoe), Nb (8 to 13%) and Th (8 to 19% in the Temnoe Lake
495 and up to 50% in the Ilasskoe Bog). These effects were mostly pronounced in the Temnoe Lake
496 in June and August and in peatland pool of the Ilasskoe Bog (July).

497

498 **4. Discussion**

499 *4.1. Comparison between biodegradation and photolysis*

500 The impact of season on the biodegradable DOC could be tested only for Lake Temnoe
501 because it was sampled during the 3 main hydrological periods. The maximal biodegradation of
502 the lake water was observed during autumn, when large amount of labile fresh soil OM and plant
503 litter were delivered to the lake from the watershed via surface runoff. The water temperature
504 seems to be of secondary importance for the intensity and rate of DOM biodegradation. This is
505 also confirmed by lack of statistically significant (at $p < 0.05$) correlation between water

506 temperature and BDOC parameters (overall magnitude and rate). It is worth noting that the
507 seasonal pattern of BDOC in the humic lake quantified in this study (**Fig. 4 A**) contrasted with
508 previous works on biodegradation of large Arctic streams and rivers whose BDOC decreased as
509 the Arctic summer progressed (Vonk et al., 2015). Presumably, the input of fresh plant litter from
510 the forested watershed of Lake Temnoe provided elevated biodegradation in the water column at
511 the end of the open water season. Another reason could be due to lake overturn in October and
512 exposure of deep, partially autochthonous, and thus biodegradable, DOM to the surface horizons.
513 A supply of limiting nutrients (N and P) to the upper 0-10 m layer during lake overturn could
514 also promote such biodegradation in October.

515 The highest biodegradation rates in the uppermost sections of the bog hydrological
516 continuum (piezometer, **Fig. 3 A**) are consistent with recent findings on organic-rich waters of
517 permafrost peatlands (Shirokova et al., 2019; Payandi-Rolland et al., 2020) and earlier results on
518 headwaters, small streams and soil leachates (Roehm et al., 2009; Ilina et al., 2014; Mann et al.,
519 2014, 2015; Larouche et al., 2015; Spencer et al., 2015; Vonk et al., 2015; Moody et al., 2013;
520 Pickard et al., 2017; Dean et al., 2019). This could be due to the very short water residence time
521 and freshly leached DOM in these water objects (i.e., Mann et al., 2012; Abbott et al., 2014;
522 Payandi-Rolland et al., 2020), given that bioavailable DOM components leached from plant litter
523 are rapidly utilized (Textor et al., 2018). At the same time, overly low BDOC (2-8 %) values,
524 regardless of depth and season in humic lake and across the hydrological continuum of the bog
525 (**Fig. 2 A**), are supportive of previous results for permafrost peatlands from the neighboring
526 region (Shirokova et al., 2019). A general path for DOM spectral properties modification over
527 the course of biodegradation consisted of an increase in aromaticity of DOM due to preferential
528 uptake of non-humic low molecular weight (LMW) compounds. However, this was not
529 accompanied by an increase in SUVA (**Fig. S3**). Presumably, the proportion of these compounds
530 in the overall DOC level was quite low and could not impact SUVA evolution. Globally, the

531 evolution of optical ratios was consistent with bacterial consumption of aliphatic LMW
532 compounds and an increase in the overall aromaticity of DOM.

533 Concerning the seasonal variation of photodegradation in the deep humic lake, maximal
534 effects were observed in June. These effects likely occurred due to fresh terrestrial organic matter
535 leached from the watershed and then efficiently processed during Arctic summer. It should be
536 noted that labile phenolic, carbohydrates, N-containing bases and smaller molecular weight
537 compounds are abundant in litter leachates produced during initial decay stages (Kiikkilä et al.,
538 2011, 2012, 2013; Hensgens et al., 2021). By July, most of the biodegradable DOM was already
539 removed, and in October, the effects were much lower. Therefore, photolabile DOM is delivered
540 from the forested watershed to the lake essentially during surface flux, at high water flow. It is
541 then quickly removed from the water column, which was especially seen in the 0.5 and 5 m
542 horizons of Lake Temnoe. Although labile organic matter from litter fall was also delivered
543 during autumn rain season, presumably, during this period, the conditions for photolysis (low
544 temperature, short daytime period and insufficient light) were not as favorable as those in June
545 or August.

546 Photodegradation of waters from the Ilaskoe Bog continuum demonstrated maximal
547 rates in soil waters from the piezometer (**Fig. 3 B**). During photolysis of humic water, a decrease
548 in optical ratios ($E_{365}:E_{470}$; $E_{470}:E_{665}$) clearly indicated preferential degradation of humic aromatic
549 compounds. The strong effect of photodegradation on DOM optical properties in the 650-500
550 nm region may be linked to decomposition of complex DOM into smaller molecules, whereas a
551 decrease of absorbance in the 230-400 nm region (**Fig. S8**) indicates degradation of aromatic
552 compounds, progressively increasing over insolation time. A recent study of DOM photolysis in
553 humic-rich forested streams demonstrated that high aromatic material was photochemically
554 converted into smaller non-fluorescent molecules (Wilske et al., 2020).

555 Results obtained on the more important role of photodegradation over biodegradation are
556 generally consistent with earlier reports on the dominance of photolysis for DOM processing in
557 Arctic waters within North America (Cory et al., 2014; Ward et al., 2017), the Canadian
558 temperate zone (Winter et al., 2007; Porcal et al., 2013, 2014, 2015), and Swedish headwater
559 catchments (Köhler et al., 2002). According to former results for Scandinavian surface waters,
560 the main impact of DOM photolysis is reflected by a decrease in the proportion of aromatic
561 (colored) DOC and a rather small ($\leq 10\%$) change in bulk DOC concentration (Groeneveld et
562 al., 2016; Koehler et al., 2014), Canada (Laurion and Mladenov, 2013; Gareis and Lesack, 2018)
563 and NW Russia (Oleinikova et al., 2017; Chupakova et al., 2018).

564 As a further perspective of this work, one has to consider biodegradation of photolytically
565 altered DOM given that photo-oxidation is known to transform molecular structures into more
566 bioavailable forms (e.g., Cory and Kling, 2018; Sulzberger et al., 2019) thereby stimulating
567 microbial growth under sunlight, as is known for other Arctic and subarctic settings (i.e.,
568 Drozdova et al., 2020; Laurion et al., 2020).

569

570 *4.2. Possible impact of microbial and photolytic processing on CO₂ emissions from* 571 *water surfaces*

572 The integral rates of DOM bioprocessing in the water column of Lake Temnoe (**Table 3,**
573 **Fig. 4 A**) allow quantifying the potential contribution of biodegradation to CO₂ production and
574 emission. Assuming all biodegraded DOM is transformed into CO₂ and there is no biomass
575 increase or sedimentation, a 1 m water layer of the lake can emit 1.7 mmol CO₂ m⁻² d⁻¹ in June
576 and 3.3 mmol CO₂ m⁻² d⁻¹ in October. Therefore, integral flux from 10 m deep water layer
577 amounts to 17 – 33 mmol CO₂ m⁻² d⁻¹ across the seasons. These values are comparable to typical
578 values of CO₂ evasion from the surface of this lake during different seasons (30-70 mmol CO₂
579 m⁻² d⁻¹; **Table 1 B**). For surface waters of Ilasskoe Bog, maximal CO₂ production due to DOM

580 biomineralization alone (**Table 3**) ranged from 5.0 mmol CO₂ m⁻² d⁻¹ for the peatland pool (2 m
581 deep) to 2.5 mmol CO₂ m⁻² d⁻¹ for the outlet stream (0.5 m deep). However, in summer, the
582 peatland pool and stream emitted 23 and 150 mmol CO₂ m⁻² d⁻¹ (**Table 1 A**) which could not be
583 sustained by DOM biodegradation.

584 The addition of photodegradation (assuming a photic layer depth of 3.5 m) to DOM
585 bioprocessing in the water column of the Temnoe Lake during open water season can further
586 increase potential CO₂ production in the water column. For the case of Ilasskoe Bog waters, the
587 addition of photolytic degradation increases projected CO₂ emission from the outlet stream by a
588 factor of 5, which is still below the actual CO₂ flux, whereas DOM photolysis has no impact on
589 CO₂ emissions from the peatland pool. Note that, although the depth of sunlight processing in
590 boreal waters is typically 1-0.8 m (Vähätalo et al., 2000; Koehler et al., 2014), a more recent
591 study concluded that direct photomineralization of DOM in Arctic humic ponds is limited to the
592 first centimeters of the water column (Mazoyer et al., 2022). Furthermore, in typical DOM-rich
593 Arctic waters, only half of sunlight-associated DOC losses is converted into CO₂ and the rest
594 may be turned into particles through photoflocculation (e.g., Mazoyer et al., 2022). Therefore,
595 despite a faster photodegradation rate compared to biodegradation, due to the shallow photic
596 layer in humic waters, the biodegradation may provide the largest impact on CO₂ emission from
597 the water column of boreal waters.

598 At the same time, our assumption that all CO₂ in lake water is produced by bio- or
599 photodegradation of DOM might not be warranted because there are multiple sources of CO₂ in
600 the lake waters, which were not assessed in the present study. These including but not limited to:
601 particulate organic matter bio- and photodegradation, whose importance can strongly exceed that
602 of DOC (e.g., Attermeyer et al., 2018; Keskitalo et al., 2022), sediment respiration, plankton and
603 periphyton diel photosynthetic cycle, underground water discharge at the lake bottom, and
604 delivery of DOC and CO₂-rich waters via lateral surface and shallow subsurface influx. Given

605 that the contribution of each CO₂ source can vary among different water bodies and across
606 seasons, the assessment of DOM bio- and photodegradation contribution to overall CO₂ flux in
607 this study should be considered as highly conservative.

608

609 *4.3. Impact of DOM bio- and photo transformation on trace element pattern*

610 In this study we hypothesized the following link between DOC and TE: in humic surface
611 waters of peatlands, most TE, which include divalent transition metals (Cu, Ni, Co, Zn, Mn),
612 toxicants (Be, Cr, Cd, Pb), trivalent and tetravalent hydrolysates (Al, Ga, Y, REE, Ti, Zr, Hf,
613 Th), with an exception of some alkalis and oxyanions, are strongly (> 80%) associated to DOM
614 in the form of organic, organo-ferric and organo-aluminium colloids (Pokrovsky et al., 2012,
615 2016). As a result, any DOM transformation processes, be it bio- or photo-degradation, may
616 directly affect the concentration pattern of TE. Specifically, removal of DOM via photo- or bio-
617 degradation should change the speciation of those elements, that are strongly bound to DOM
618 such as divalent transition metals, or incorporated into organo-mineral (Fe, Al) colloids, such as
619 trivalent and tetravalent hydrolysates (TE³⁺, TE⁴⁺). The former might either remain in solution
620 (during photodegradation), hence not modifying their total dissolved concentration, or being
621 taken up by growing bacteria during bio-degradation. The latter (TE³⁺, TE⁴⁺) are capable of co-
622 precipitating with Fe and Al hydroxides, especially during photodegradation (i.e., Kopacek et al.,
623 2005, 2006), hence being sizably removed from the aqueous solution. From the other hand, some
624 TE are known to be photosensitive (Mn, Fe), toxic (Al, Cu, As, Cd, Pb), or potentially limiting
625 micronutrients (Zn, Co, Ni, Mo) for the bacteria and therefore they are capable affecting the
626 overall rate of photo- or bio-degradation.

627 However, contrary to our expectations, among all major and trace elements measured in
628 the experiments, only trivalent and tetravalent hydrolysates (TE³⁺, TE⁴⁺) were impacted by both
629 photo- and biodegradation. It is known that these elements are essentially present in the form of

630 large molecular size, highly polymerized and presumably aromatic, organo-Fe/Al colloids in
631 humic boreal/subarctic lakes (Pokrovsky et al., 2012, 2016), rivers (Krickov et al., 2019;
632 Pokrovsky et al., 2010), and soil porewaters (Pokrovsky et al., 2005; Raudina et al., 2021).
633 Therefore, insoluble TE^{3+} and TE^{4+} generally followed the removal of Fe(III) in the form of
634 particulate Fe hydroxides, after breaking the Fe-DOM bonds that stabilized colloidal Fe(III)
635 hydroxides. This destabilization and Fe hydroxide particle formation is known to occur either via
636 biodegradation (i.e., Oleinikova et al., 2018) or photolysis (Kopacek et al., 2005, 2006;
637 Oleinikova et al., 2017; Chupakova et al., 2018). At the same time, some micronutrients (V, Mn,
638 Co, Cu and Ba) were affected solely by biodegradation. This can reflect uptake of these metals
639 by growing bacterial cells, as is known from laboratory experiments with pure cultures of
640 heterotrophic bacteria (Shirokova et al., 2017a).

641 Note that the effects of bio- and photodegradation were more pronounced for light REE
642 (LREE) compared to heavy REE (HREE). This result is consistent with the fact that LREE have
643 stronger association with Fe hydroxide compared to organic complexes, as known from general
644 chemical considerations and laboratory experiments (i.e., Bau, 1999) and evidenced in various
645 boreal and subarctic settings (Pokrovsky et al., 2016; Krickov et al., 2019). Given that the main
646 effect of both photolysis and biodegradation of DOM in humic Fe(III)-rich surface waters is
647 coagulation of dissolved Fe(III) in the form of Fe oxy(hydr)oxides, the LREE are removed from
648 solution. This removal occurs in the form of adsorbed complexes or coprecipitated with Fe
649 oxy(hydr)oxides, while HREE remain in the form of strong aqueous complexes.

650 In former studies of photo- and biodegradation of surface waters from permafrost
651 peatlands, only a few nutrients (P, Fe, Zn and V) and insoluble low mobility trace metals (Ti, Zr,
652 Nb and Th) demonstrated a decrease in concentration (Shirokova et al., 2019). This list of
653 elements is generally consistent with that established in the present study of humic subarctic
654 lakes of the non-permafrost zone, except P and Zn which did not exhibit sizable removal in our

655 experiments. It is possible that a high proportion of low molecular weight $LMW_{< 1 \text{ kDa}}$ (and thus,
656 potentially bioavailable) forms of macro- and micronutrients, such as P and Zn, in the permafrost
657 ice (i.e., Kuzmina et al., 2023) can be delivered to the lake and river via suprapermafrost flow
658 (Raudina et al., 2018, 2021). This led to elevated bioavailability of these elements in permafrost
659 surface waters reported in previous works, as compared to permafrost-free boreal settings of this
660 study.

661

662 **Conclusions**

663 Seasonally resolved bio- and photo-degradability of DOM in a deep stratified lake and
664 summer measurements from a peat bog's hydrological continuum within the boreal zone
665 confirmed the initial hypothesis that the subsurface and deep horizons of these stratified waters
666 are mostly sensitive to sunlight impact, and that maximal effects of photodegradation occurred
667 in the month of June during strong insolation. In contrast, the biodegradation of DOM from the
668 humic lake was mostly pronounced during October, when fresh leachates of forest litter were
669 exported from the watershed. The evolution of optical parameters of DOM demonstrated removal
670 of aliphatic, presumably autochthonous organic ligands during biodegradation and photolysis.
671 Insoluble, low-mobility trace metals such as trivalent and tetravalent hydrolysates were affected
672 by both bio- and photodegradation, as they are associated with coagulating Fe(III)
673 oxyhydroxides. A few micronutrients (V, Mn, Co, Cu and Ba) were, however, removed during
674 biodegradation experiments, thus reflecting their possible uptake by microorganisms.

675 Although DOM photodegradation rates were sizably higher compared to those of
676 biodegradation, the rather thin photic layer in humic waters does not allow for significant
677 contribution of photolysis in overall CO_2 emission from lake and bog surfaces. In the deep
678 stratified lake, the biodegradation alone was capable explaining observed CO_2 emissions, while
679 in the shallow bog continuum, the sum of bio- and photodegradation were not sufficient to

680 provide CO₂ flux, hence suggesting additional source of CO₂ such as subsurface water influx
681 from peat layers. The high seasonal dynamics and spatial variability in both photo- and
682 biodegradability of DOM and related trace elements of humic surface waters in the boreal zone
683 encountered in this study suggest the need for further assessment of rates of these processes with
684 focus on early spring and late autumn, the periods of maximal photo- and biodegradation,
685 respectively. Considering the strong spatial variations of DOM processing in the aquatic
686 continuum, focus should be centered on the most dynamic components such as small streams and
687 subsurface waters, which demonstrated the highest rates of both photo- and biodegradation.

688

689 **Acknowledgements**

690 This work was supported by RSF grant No 22-17-00253. LS and OP were also supported
691 by project PEACE of PEPR FairCarboN ANR-22-PEXF-0011. OP is grateful for partial support
692 from the TSU Development Programme Priority-2030.

693

694 **Assets:** All the data obtained in this work are presented in Supplementary Information file.

695

696 **Authors contribution.**

697 AVC and OP designed the study and wrote the paper; AC, NN and SB performed sampling,
698 analysis and their interpretation; LS performed bacterial number assessment and DOC results
699 interpretation; AVC, TV and OP provided analyses of literature data.

700

701 **Competing interests.**

702 The authors declare that they have no conflict of interest.

703

704

705

706 **References**

- 707 Abbott, B. W., Larouche, J. R., Jones, J. B., Bowden, W. B., and Balsler, A. W.: Elevated
708 dissolved organic carbon biodegradability from thawing and collapsing permafrost, *J.*
709 *Geophys. Res.*, 119, 2049–2063, 2014.
- 710 Amado, A. M., Cotner, J. B., Cory, R. M., Edhlund, B. L., and McNeill, K.: Disentangling the
711 interactions between photochemical and bacterial degradation of dissolved organic matter:
712 amino acids play a central role, *Microb. Ecol.*, 69(3), 554-566, 2014.

713 Amaral, V., Ortega, T., Romera-Castillo, C., and Forja, J.: Linkages between greenhouse gases
714 (CO₂, CH₄, and N₂O) and dissolved organic matter composition in a shallow estuary, *Sci.*
715 *Total Environ.* 788, Art No 147863, 2021.

716 Andersson, M. G. I., Catalán, N., Rahman, Z., Tranvik, L. J., and Lindström, E. S.: Effects of
717 sterilization on dissolved organic carbon (DOC) composition and bacterial utilization of
718 DOC from lakes, *Aquat. Microb. Ecol.*, 82, 199-208, 2018.

719 Ask, J., Karlsson, J., and Jansson, M.: Net ecosystem production in clear-water and brown-water
720 lakes, *Glob. Biogeochem. Cycles*, 26, GB1017, doi:10.1029/2010GB003951, 2012.

721 Attermeyer, K., Catalán, N., Einarsdottir, K., Freixa, A., Groeneveld, M., Hawkes, J. A., et al.:
722 Organic carbon processing during transport through boreal inland waters: Particles as
723 important sites, *J. Geophys. Res.: Biogeosciences*, 123(8), 2412–2428.
724 <https://doi.org/10.1029/2018jg004500>, 2018.

725 Bau, M.: Scavenging of dissolved yttrium and rare earths by precipitating iron oxyhydroxide:
726 experimental evidence for Ce oxidation, Y-Ho fractionation, and lanthanide tetrad effect,
727 *Geochim. Cosmochim. Ac.*, 63, 67–77, 1999.

728 Battin T.J. Dissolved organic materials and its optical properties in a blackwater tributary of the
729 upper Orinoco River, Venezuela, *Organic Geochemistry*, 28, 561-569, 1998.

730 Begum, M. S., Park, J.-H., Yang, L., Shin, K. H., and Hur, J.: Optical and molecular indices of
731 dissolved organic matter for estimating biodegradability and resulting carbon dioxide
732 production in inland waters: A review. *Water Research*, Art No 119362, 2022.

733 Berggren, M., Laudon, H., and Jansson, M.: Landscape regulation of bacterial growth efficiency
734 in boreal freshwaters, *Global Biogeochem. Cy.*, 21, GB4002.
735 <http://dx.doi.org/10.1029/2006GB002844>, 2007.

736 Berggren, M., Laudon, H., Haei, M., Ström, L., and Jansson, M.: Efficient aquatic bacterial
737 metabolism of dissolved low-molecular-weight compounds from terrestrial sources, *ISME*
738 *J.*, 4, 408-416, 2010.

739 Borges, A., Darchambeau, F., Teodoru, C. et al. : Globally significant greenhouse-gas emissions
740 from African inland waters, *Nature Geosci.*, 8, 637–642. <https://doi.org/10.1038/ngeo2486>,
741 2015.

742 Chaudhary, N., Westermann, S., Lamba, S., et al.: Modelling past and future peatland
743 carbon dynamics across the pan- Arctic, *Glob. Change Biol.*, 26, 4119-4133, 2020.

744 Chin, Y.-P., Aiken, G., and O'Loughlin, E.: Molecular weight, polydispersity, and spectroscopic
745 properties of aquatic humic substances, *Environ. Sci. Technol.*, 28, 1853-1858, 1994.

746 Chupakov, A., Ershova, A., Moreva, O. Yu, Shirokova, L. S., Zabelina, S. A., Vorobieva, T.Ya.,
747 Klimov, S. I., Brovkon N., Pokrovsky, O.S.: Seasonal dynamics of dissolved carbon in
748 contrasting stratified lakes of the subarctic, *Boreal Environ. Res.*, 22, 213–230, 2017.

749 Chupakova, A. A., Chupakov, A. V., Neverova, N. V., Shirokova, L. S., and Pokrovsky, O. S.:
750 Photodegradation of river dissolved organic matter and trace metals in the largest European
751 Arctic estuary, *Sci. Total Environ.*, 622–623, 1343–1352, 2018.

752 Cole, J. J. and Caraco, N.: Atmospheric exchange of carbon dioxide in a low-wind oligotrophic
753 lake measured by the addition of SF₆, *Limnol. Oceanog.*, 43, 647–656, 1998.

754 Cole, J. J., Prairie, Y. T., Caraco, N. F., McDowell, W. H., Tranvik, L. J., Striegl, R. G., Duarte,
755 C. M., Kortelainen, P., Downing, J. A., Middelburg, J. J., and Melack, J.: Plumbing the
756 global carbon cycle: Integrating inland waters into the terrestrial carbon budget, *Ecosystems*,
757 10, 172–185, <https://doi.org/10.1007/s10021-006-9013-8>, 2007.

758 Cory, R. M., Ward, C. P., Crump, B. C., and Kling, G. W.: Sunlight controls water column
759 processing of carbon in arctic fresh waters, *Science*, 345, 925-928, 2014.

760 Cory, R. M., and Kling, G. W.: Interactions between sunlight and microorganisms influence
761 dissolved organic matter degradation along the aquatic continuum, *Limnol. Oceanogr. Lett.*,
762 3, 102–116, 2018.

763 Dean, J. F., van Hal, J. R., Dolman, A. J., Aerts, R., and Weedon, J. T.: Filtration artefacts in
764 bacterial community composition can affect the outcome of dissolved organic matter
765 biolability assays, *Biogeosciences*, 15, 7141-7154, [https://doi.org/10.5194/bg-15-7141-](https://doi.org/10.5194/bg-15-7141-2018)
766 2018, 2018.

767 Dean, J. F., Garnett, M. H., Spyrakos, E., Billett, M. F.: The potential hidden age of dissolved
768 organic carbon exported by peatland streams, *J. Geophys. Res.: Biogeosciences*,
769 124, 328–341, 2019.

770 Don, A., and Kalbitz, K.: Amount and degradability of dissolved organic carbon from foliar litter
771 at different decomposition stages, *Soil Biol. Biochem.*, 37, 2171-2179, 2005.

772 Drozdova, O. Y., Aleshina, A. R., Tikhonov, V. V., Lapitskiy, S. A., and Pokrovsky, O. S.:
773 Coagulation of organo-mineral colloids and formation of bioavailable low molecular weight
774 organic complexes in boreal humic river water under UV-irradiation, *Chemosphere*, 250,
775 Art No 126216, doi.org/10.1016/j.chemosphere.2020.126216, 2020.

776 Gareis, J. A. L., and Lesack, L. F. W.: Photodegraded dissolved organic matter from peak
777 freshet river discharge as a substrate for bacterial production in a lake-rich great Arctic delta,
778 *Arctic Science*, 4(4), 557-583, 2018.

779 Groeneveld, M., Tranvik, L., Natchimuthu, S., and Koehler, B.: Photochemical mineralisation in
780 a boreal brown water lake: considerable temporal variability and minor contribution to
781 carbon dioxide production, *Biogeoscience*, 13, 3931-3943, 2016.

782 Harris, L. I., Richardson, K., Bona, K. A., Davidson, S. J., Finkelstein, S. A., Garneau, M.,
783 McLaughlin, J., Nwaishi, F., Olefeldt, D., Packalen, M., Roulet, N. T., Southee, F. M.,
784 Strack, M., Webster, K. L., Wilkinson, S. L., and Ray, J. C.: The essential carbon service
785 provided by northern peatlands, *Front. Ecol. Environ.*, 20, 222–230,
786 <https://doi.org/10.1002/fee.2437>, 2022.

787 Hengsgens, G., Lechtenfeld, O. J., Guillemette, F., Laudon, H., Berggren, M.: Impacts of litter
788 decay on organic leachate composition and reactivity, *Biogeochemistry* 154, 99-117, 2021.

789 Hiriart-Baer, V.P., Diep, N., and Smith, R.E.H.: Dissolved organic matter in the Great Lakes: role
790 and nature of allochthonous material, *J. Great Lakes Res.* 34, 383–394, 2008.

791 Hur, J., Williams, M. A., and Schlautman, M. A.: Evaluating spectroscopic and chromatographic
792 techniques to resolve dissolved organic matter via end member mixing analysis, *Chemosphere*,
793 63, 387-402, 2006.

794 Ilina, S. M., Drozdova, O. Yu., Lapitsky, S. A., Alekhin, Yu. V., Demin, V. V., Zavgorodnaya, Yu.
795 A., Shirokova, L. S., Viers, J., and Pokrovsky, O. S.: Size fractionation and optical properties
796 of dissolved organic matter in the continuum soil solution-bog-river and terminal lake of a
797 boreal watershed, *Org. Geochem.*, 66, 14–24, 2014.

798 Kalbitz, K., Schmerwitz, J., Schwesig, D., and Matzner, E.: Biodegradation of soil-derived
799 dissolved organic matter as related to its properties, *Geoderma* 113, 273-291, 2003.

800 Karlsson, J., Serikova, S., Rocher-Ros, G., Denfeld, B., Vorobyev, S. N., Pokrovsky, O. S.:
801 Carbon emission from Western Siberian inland waters, *Nature Comm.*, 12, 825,
802 <https://doi.org/10.1038/s41467-021-21054-1>, 2021.

803 Kawahigashi, M., Kaiser, L., Kalbitz, K., Rodionov, A., and Guggenberger, G.: Dissolved
804 organic matter in small streams along a gradient from discontinuous to continuous
805 permafrost. *Global Change Biol.* 10, 1576-1586, 2004.

806 Keskitalo, K.H., Bröder, L., Jong, D., Zimov, N., Davydova, A., Davydov, S., Tesi, T., Mann, P.
807 J., Haghypour, N., Eglinton, T. I., and Vonk, J. E.: Seasonal variability in particulate organic

808 carbon degradation in the Kolyma River, Siberia. *Environmental Research Letters*, 17(3),
809 Art No 034007. DOI 10.1088/1748-9326/ac4f8d, 2022.

810 Kiikkilä, O., Kitunen, V., and Smolander, A.: Properties of dissolved organic matter derived
811 from silver birch and Norway spruce stands: Degradability combined with chemical
812 characteristics, *Soil Biol. Biochem.* 43, 421-430, 2011.

813 Kiikkilä, O., Kitunen, V., Spetz, P., and Smolander, A.: Characterization of dissolved organic
814 matter in decomposing Norway spruce and silver birch litter, *European J Soil Sci* 63, 476-
815 486, 2012.

816 Kiikkilä, O., Smolander, A., and Kitunen, V.: Degradability, molecular weight and adsorption
817 properties of dissolved organic carbon and nitrogen leached from different types of
818 decomposing litter, *Plant Soil* 373, 787-798, 2013.

819 Koehler, B., Landelius, T., Weyhenmeyer, G. A., Machida, N., and Tranvik, L.J.: Sunlight-
820 induced carbon dioxide emissions from inland waters, *Global Biogeochem. Cycles*, 28, 696–
821 711, 2014.

822 Köhler, S., Buffam, I., Jonsson, A., and Bishop, K.: Photochemical and microbial processing of
823 stream and soil water dissolved organic matter in a boreal forested catchment in northern
824 Sweden, *Aquat. Sci.*, 64, 269–281, 2002.

825 Kopáček, J., Klementova, S., and Norton S. A.: Photochemical production of ionic and
826 particulate aluminum and iron in lakes, *Environ. Sci. Technol.*, 39, 3656–3662, 2005.

827 Kopáček, J., Marešová, M., Norton, S. A., Porcal, P., and Veselý, J.: Photochemical source of
828 metals for sediments, *Environ. Sci. Technol.*, 40(14), 4455–4459.
829 <https://doi.org/10.1021/es0600532>, 2006.

830 Krickov, I. V., Pokrovsky, O. S., Manasypov, R. M., Lim, A., Shirokova, L. S., and Loiko, S.
831 V.: Colloidal transport of carbon and metals by western Siberian rivers during different
832 seasons across a permafrost gradient, *Geochim. Cosmochim. Acta* 265, 221-241,
833 <https://doi.org/10.1016/j.gca.2019.08.041>, 2019.

834 Kuzmina, D., Lim, A. G., Loiko, S. V., Shirokova, L. S., Julien, F., Rols, J. L., and Pokrovsky,
835 O. S.: Dispersed ice of permafrost peatlands represents an important source of labile
836 carboxylic acids, nutrients and metals, *Geoderma*, 429, Art No 116256.
837 <https://doi.org/10.1016/j.geoderma.2022.116256>, 2023.

838 Lapierre, J.-F., Guillemette, F., Berggren, M., and del Giorgio, P. A.: Increases in terrestrially
839 derived carbon stimulate organic carbon processing and CO₂ emissions in boreal aquatic
840 ecosystems, *Nature Comm.*, 4, 2972, doi:10.1038/ncomms3972, 2013.

841 Larouche, J. R., Abbott, B. W., Bowden, W. B., Jones, and J. B.: The role of watershed
842 characteristics, permafrost thaw, and wildfire on dissolved organic carbon biodegradability
843 and water chemistry in Arctic headwater streams, *Biogeosciences*, 12, 4221-4233, 2015.

844 Lau, M. P.: Linking the dissolved and particulate domain of organic carbon in inland waters. *J.*
845 *Geophys. Res.: Biogeosciences*, 126, e2021JG006266.
846 <https://doi.org/10.1029/2021JG006266>, 2021.

847 Laurion, I., and Mladenov, N.: Dissolved organic matter photolysis in Canadian Arctic thaw
848 ponds, *Environ. Res. Lett.*, 8, 035026, doi.org/10.1088/1748-9326/8/3/035026, 2013.

849 Laurion, I., Massicotte, P., Mazoyer, F., Negandhi, K., and Mladenov, N.: Weak mineralization
850 despite strong processing of dissolved organic matter in Eastern Arctic tundra ponds,
851 *Limnol. Oceanogr.*, 66, S47–S63, <https://doi.org/10.1002/lno.11634>, 2021.

852 Liu, F., and Wang, D.: Dissolved organic carbon concentration and biodegradability across the
853 global rivers: A meta-analysis, *Sci. Total Environ.*, 818, Art No 151828, 2022.

854 Lou, T., and Xie, H.: Photochemical alteration of the molecular weight of dissolved organic
855 matter, *Chemosphere*, 65, 2333-2342, 2006.

856 Mann, P. J., Davydova, A., Zimov, N., Spencer, R. G. M., Davydov, S., Bulygina, E., Zimov, S.,
857 Holmes, R. M.: Controls on the composition and lability of dissolved organic matter in
858 Siberia's Kolyma River basin, *J. Geophys. Res.*, 117, G01028, doi: 10.1029/2011JG001798,
859 2012.

860 Mann, P. J., Sobczak, W. V., LaRue, M. M., Bulygina, E., Davydova, A., Vonk, J. E., Schade,
861 J., Davydov, S., Zimov, N., Holmes, R. M., Spencer, R. G. M.: Evidence for key enzymatic
862 controls on metabolism of Arctic river organic matter, *Global Change Biol.*, 20(4), 1089-
863 1100, 2014.

864 Mann, P. J., Eglinton, T. I., McIntyre, C. P., Zimov, N., Davydova, A., Vonk, J. E., Holmes, R.
865 M., Spencer, R. G. M.: Utilization of ancient permafrost carbon in headwaters of Arctic
866 fluvial networks, *Nat. Commun.*, 6, doi: 10.1038/ncomms8856, 2015.

867 Mazoyer, F., Laurion, I., and Rautio, M.: The dominant role of sunlight in degrading winter
868 dissolved organic matter from a thermokarst lake in a subarctic peatland, *Biogeosciences*,
869 19, 3959–3977, <https://doi.org/10.5194/bg-19-3959-2022>, 2022.

870 Moody, C. S., Worrall, F., Evans, C. D., Jones, T. G.: The rate of loss of dissolved organic carbon
871 (DOC) through a catchment, *J. Hydrol.*, 492, 139-150, 2013.

872 Moran, M. A., Sheldon, W. M., and Zepp, R. G.: Carbon loss and optical property changes during
873 long-term photochemical and biological degradation of estuarine dissolved organic matter,
874 *Limnol. Oceanogr.*, 45, 1254–1264, 2000.

875 Mostofa, K. M. G., Yoshioka, T., Konohira, E., and Tanoue, E.: Photodegradation of fluorescent
876 dissolved organic matter in river waters, *Geochem. J.*, 41, 323-331, 2007.

877 Obernosterer, I., and Benner, R.: Competition between biological and photochemical processes
878 in the mineralization of dissolved organic carbon, *Limnol. Oceanogr.*, 49, 117–124,
879 <https://doi.org/10.4319/lo.2004.49.1.0117>, 2004.

880 Oleinikova, O., Drozdova, O. Y., Lapitskiy, S. A., Bychkov, A. Y., and Pokrovsky, O. S.:
881 Dissolved organic matter degradation by sunlight coagulates organo-mineral colloids and
882 produces low-molecular weight fraction of metals in boreal humic waters, *Geochim.
883 Cosmochim. Acta*, 211, 97-114, 2017.

884 Oleinikova, O., Shirokova, L. S., Drozdova, O. Y., Lapitsky, S. A., and Pokrovsky, O. S.: Low
885 biodegradability of dissolved organic matter and trace metal from subarctic waters by culturable
886 heterotrophic bacteria, *Sci. Total Environ.*, 618, 174-187, 2018.

887 Payandi-Rolland, D.; Shirokova, L.S.; Tesfa, M.; Lim, A.G.; Kuzmina, D.; Benezeth, P.;
888 Karlsson, J.; Giesler, R.; Pokrovsky, O.S.: Dissolved organic matter biodegradation along a
889 hydrological continuum in a discontinuous permafrost area: Case study of northern Siberia
890 and Sweden, *Sci. Total Environ.*, 749, Art No 141463, 2020.

891 Peacock, M., Evans, C. D., Fenner, N., Freeman, C., Gough, R., Jones, T. G., and Lebron, I.:
892 UV-visible absorbance spectroscopy as a proxy for peatland dissolved organic carbon
893 (DOC) quantity and quality: considerations on wavelength and absorbance degradation,
894 *Environmental Science: Processes and Impacts*, 10–12, doi:10.1039/c4em00108g, 2014.

895 Pickard, A. E., Heal, K. V., McLeod, A. R., and Dinsmore, K. J.: Temporal changes in
896 photoreactivity of dissolved organic carbon and implications for aquatic carbon fluxes from
897 peatlands, *Biogeosciences*, 14, 1793-1809, <https://doi.org/10.5194/bg-14-1793-2017>, 2017.

898 Pokrovsky, O. S., Dupré, B., and Schott, J.: Fe-Al-organic colloids control the speciation of trace
899 elements in peat soil solutions: results of ultrafiltration and dialysis, *Aquatic Geochem.*, 11,
900 241-278, 2005.

901 Pokrovsky, O. S., Viers, J., Shirokova, L. S., Shevchenko, V. P., Filipov, A. S., and Dupré, B.:
 902 Dissolved, suspended, and colloidal fluxes of organic carbon, major and trace elements in
 903 Severnaya Dvina River and its tributary, *Chem. Geol.*, 273, 136–149, 2010.

904 Pokrovsky, O. S., Shirokova, L. S., Zabelina, S. A., Vorobieva, T. Ya., Moreva, O. Yu., Klimov,
 905 S. I., Chupakov, A. V., Shorina, N. V., Kokryatskaya, N. M., Audry, S., Viers, J., Zoutien,
 906 C., and Freyrier, R.: Size fractionation of trace elements in a seasonally stratified boreal
 907 lakes: Control of organic matter and iron colloids, *Aquat. Geochem.*, 18, 115–139, 2012.

908 Pokrovsky, O. S., Manasypov, R. M., Loiko, S. V., and Shirokova, L. S.: Organic and organo-
 909 mineral colloids of discontinuous permafrost zone, *Geochim. Cosmochim. Ac.*, 188, 1–20,
 910 2016.

911 Porcal, P., Dillon, P. J., and Molot, L. A.: Photochemical production and decomposition of
 912 particulate organic carbon in a freshwater stream, *Aquat. Sci.*, 75, 469–482, 2013.

913 Porcal, P., Dillon, P. J., and Molot, L. A.: Interaction of extrinsic chemical factors affecting
 914 photodegradation of dissolved organic matter in aquatic ecosystems, *Photochem. Photobiol.*
 915 *Sci.*, 13, 799–812, 2014.

916 Porcal, P., Dillon, P. J., and Molot, L. A.: Temperature dependence of photodegradation of
 917 dissolved organic matter to dissolved inorganic carbon and particulate organic carbon, *Plos*
 918 *ONE*, 10(6), e0128884, DOI:10.1371/journal.pone.0128884, 2015.

919 Prijac, A., Gandois, L., Jeanneau, L., Taillardat, P., and Garneau, M.: Dissolved organic matter
 920 concentration and composition discontinuity at the peat–pool interface in a boreal peatland,
 921 *Biogeosciences*, 19, 4571–4588, <https://doi.org/10.5194/bg-19-4571-2022>, 2022.

922 Raudina, T. V., Loiko, S. V., Lim, A., Manasypov, R. M., Shirokova, L. S., Istigecev, G. I.,
 923 Kuzmina, D. M., Kulizhsky, S. P., Vorobyev, S. N., and Pokrovsky, O. S.: Permafrost thaw
 924 and climate warming may decrease the CO₂, carbon, and metal concentration in peat soil
 925 waters of the Western Siberia Lowland, *Sci. Total Environ.*, 634, 1004–1023, 2018.

926 Raudina, T. V., Loiko, S., Kuzmina, D. M., Shirokova, L. S., Kulizhsky, S. P., Golovatskaya, E.
 927 A., and Pokrovsky, O. S.: Colloidal organic carbon and trace elements in peat porewaters
 928 across a permafrost gradient in Western Siberia, *Geoderma* 390, Art No 114971,
 929 <https://doi.org/10.1016/j.geoderma.2021.114971>, 2021.

930 Raudina, T. V., Smirnov, S. V., Luschaeva, I. V., Kulizhskiy, S. P., Golovatskaya, E. A.,
 931 Shirokova, L.S., and Pokrovsky, O. S.: Seasonal and spatial variations of dissolved organic
 932 matter biodegradation along the aquatic continuum in the southern taiga bog complex,
 933 Western Siberia. *Water (MDPI)*, 14, Art No 3969. <https://doi.org/10.3390/w1423396>, 2022.

934 Roehm, C. L., Giesler, R., Karlsson, J.: Bioavailability of terrestrial organic carbon to lake
 935 bacteria: The case of a degrading subarctic permafrost mire complex, *J. Geophys. Res.*, 114,
 936 G03006, doi: 10.1029/2008JG000863, 2009.

937 Rosset, T., Binet, S., Rigal, F., and Gandois, L.: Peatland dissolved organic carbon export to
 938 surface waters: Global significance and effects of anthropogenic disturbance, *Geophysical*
 939 *Res. Lett.*, 49, e2021GL096616. <https://doi.org/10.1029/2021GL096616>, 2022.

940 Selvam, B. P., Lapierre, J.-F., Guillemette, F., Voigt, C., Lamprecht, R. E., Biasi, C., Christensen,
 941 T. R., Martikainen P. J., and Berggren, M.: Degradation potentials of dissolved organic
 942 carbon (DOC) from thawed permafrost peat, *Scientific Reports*, 7, Art No 45811, doi:
 943 10.1038/srep45811, 2016.

944 Serikova, S., Pokrovsky, O. S., Ala-aho, P., Kazantsev, V., Kirpotin, S. N. Kopysov, S. G.,
 945 Krickov, I. V., Laudon, H., Manasypov, R. M., Shirokova, L. S., Sousby, C., Tetzlaff, D.,

946 and Karlsson, J.: High riverine CO₂ emissions at the permafrost boundary of Western
947 Siberia. *Nature Geoscience*, 11, 825-829, 2018.

948 Serikova, S., Pokrovsky, O. S., Laudon, H., Krickov, I. V., Lim, A. G., Manasypov, R. M., and
949 Karlsson, J.: C emissions from lakes across permafrost gradient of Western Siberia, *Nature*
950 *Comm.* 10, Art No 1552, <https://doi.org/10.1038/s41467-019-09592-1>, 2019.

951 Shirokova, L. S., Bredoire, R., Rolls, J. L., and Pokrovsky, O. S.: Moss and peat leachate
952 degradability by heterotrophic bacteria: fate of organic carbon and trace metals,
953 *Geomicrobiol. J.*, 34(8), 641-655, 2017a.

954 Shirokova, L. S., Chupakova, A. A., Chupakov, A. V., and Pokrovsky, O.S.: Transformation of
955 dissolved organic matter and related trace elements in the mouth zone of the largest
956 European Arctic river: experimental modeling, *Inland Waters*, 7(3), 272-282, 2017b.

957 Shirokova, L. S., Labouret, J., Gurge, M., Gerard, E., Zabelina, S. A., Ivanova, I. S., Pokrovsky,
958 O. S.: Impact of cyanobacterial associate and heterotrophic bacteria on dissolved organic
959 carbon and metal in moss and peat leachate: application to permafrost thaw in aquatic
960 environments, *Aquatic Geochemistry*, 23(5–6), 331–358, [https://doi.org/10.1007/s10498-](https://doi.org/10.1007/s10498-017-9325-7)
961 [017-9325-7](https://doi.org/10.1007/s10498-017-9325-7), 2017c.

962 Shirokova, L. S., Chupakov, A. V., Zabelina, S. A., Neverova, N. V., Payandi-Rolland, D.,
963 Causseraud, C., Karlsson, J., and Pokrovsky, O. S.: Humic surface waters of frozen peat
964 bogs (permafrost zone) are highly resistant to bio- and photodegradation, *Biogeosciences*,
965 16, 2511–2526, 2019.

966 Shirokova, L. S., Chupakov, A. V., Ivanova, I. S., Moreva, O. Y., Zabelina, S. A., Shutskiy, N.
967 A., Loiko S. V., Pokrovsky, O. S. Lichen, moss and peat control of C, nutrient and trace
968 metal regime in lakes of permafrost peatlands. *Science Total Environ.*, 782, Art No 146737,
969 <https://doi.org/10.1016/j.scitotenv.2021.146737>, 2021.

970 Spencer, R. G. M., Mann, P. J., Dittmar, T., Eglinton, T. I., McIntyre, C., Holmes, R. M., Zimov,
971 N., Stubbins, A.: Detecting the signature of permafrost thaw in Arctic rivers, *Geophys. Res.*
972 *Lett.*, 42, 2830-2835, 2015.

973 Stubbins, A., Spencer, R.G., Chen, H., Hatcher, P.G., Mopper, K.W., Hernes, P.J., Mwamba,
974 V., Mangangu, A.M., Wabakanghanzi, J.N., and Six, J.: Illuminated darkness: Molecular
975 signatures of Congo River dissolved organic matter and its photochemical alteration as
976 revealed by ultrahigh precision mass spectrometry. *Limnol. Oceanogr.*, 55(4), 1467-1477,
977 10.4319/lo.2010.55.4.1467, 2010.

978 Stutter, M. I., Richards, S., and Dawson, J. J. C.: Biodegradability of natural dissolved organic
979 matter collected from a UK moorland stream, *Water Res.*, 47(3), 1169-1180, 2013.

980 Sulzberger, B., Austin, A. T., Cory, R. M., Zepp, R. G., and Paul, N. D.: Solar UV radiation in
981 a changing world: roles of cryosphere-land-water-atmosphere interfaces in global
982 biogeochemical cycles, *Photochem. Photobiol. Sci.*, doi: 10.1039/c8pp90063a, 2019.

983 Taillardat, P., Bodmer, P., Deblois, C. P., Ponçot, A., Prijac, A., Riahi, K., et al. : Carbon
984 dioxide and methane dynamics in a peatland headwater stream: Origins, processes and
985 implications, *J. Geophysical Res.: Biogeosciences*, 127, e2022JG006855.
986 <https://doi.org/10.1029/2022JG006855>, 2022.

987 Textor, S. R., Guillemette, F., Zito, P. A., Spencer, R. G. M.: An assessment of dissolved
988 organic carbon biodegradability and priming in blackwater systems, *J. Geophys. Res.*
989 *Biogeosciences*, 123(9), 2998-3015, 2018.

990 Tranvik, L. J., Downing, J. A., Cotner, J. B., Loiselle, S. A., Striegl, R. G., Ballatore, T. J.,
991 Dillon, P., Finlay, K., Fortino, K., Knoll, L. B., Kortelainen, P. L., Kutser, T., Larsen, S.,
992 Laurion, I., Leech, D. M., McCallister, S. L., McKnight, D. M., Melack, J. M., Overholt,
993 E., Porter, J. A., Prairie, Y., Renwick, W. H., Roland, F., Sherman, B. S., Schindler, D. W.,

994 Sobek, S., Tremblay, A., Vanni, M. J., Verschoor, A. M., von Wachenfeldt, E., and
995 Weyhenmeyer, G. A.: Lakes and reservoirs as regulators of carbon cycling and climate,
996 *Limnol. Oceanogr.*, 54, 2298–2314, 2009.

997 Vachon, D., Lapierre, J., and del Giorgio, P. A.: Seasonality of photochemical dissolved
998 organic carbon mineralization and its relative contribution to pelagic CO₂ production in
999 northern lakes, *J. Geophys. Res.-Biogeo.*, 121, 864–878,
1000 <https://doi.org/10.1002/2015JG003244>, 2016.

1001 Vachon, D., Solomon, C. T., and del Giorgio, P. A.: Reconstructing the seasonal dynamics and
1002 relative contribution of the major processes sustaining CO₂ emissions in northern lakes,
1003 *Limnol. Oceanogr.*, 62, 706–722, <https://doi.org/10.1002/lno.10454>, 2017.

1004 Vähätalo, A. V., Salonen, K., Münster, U., Järvinen, M., and Wetzel, R. G.: Photochemical
1005 transformation of allochthonous organic matter provides bioavailable nutrients in a humic
1006 lake, *Acta Hydrobiol.*, 156, 287–314, 2003.

1007 Vähätalo, A. V. and Wetzel, R.G.: Photochemical and microbial decomposition of chromophoric
1008 dissolved organic matter during long (months-years) exposures, *Mar. Chem.*, 89, 313–326,
1009 2004.

1010 Vasyukova, E., Pokrovsky, O. S., Viers, J., Oliva, P., Dupré, B., Martin, F., and Candaudap, F.:
1011 Trace elements in organic- and iron-rich surficial fluids of boreal zone: Assessing colloidal
1012 forms via dialysis and ultrafiltration, *Geochim. Cosmochim. Acta*, 74, 449–468, 2010.

1013 Vonk, J. E., Tank, S. E., Mann, P. J., Spencer, R. G. M., Treat, C. C., Striegl, R. G., Abbott,
1014 B. W., and Wickland K. P.: Biodegradability of dissolved organic carbon in permafrost
1015 soils and aquatic systems: a meta-analysis, *Biogeosciences*, 12, 6915–6930, 2015.

1016 Ward, C. P., Nalven, S. G., Crump, B. C., Kling, G. W., and Cory, R. M.: Photochemical
1017 alteration of organic carbon draining permafrost soils shifts microbial metabolic pathways
1018 and stimulates respiration, *Nature Comm.*, 8, Art No 772, 2017.

1019 Wauthy, M., Rautio, M., Christoffersen, K. S., Forsstrom, L., Laurion, I., Mariash, H. L.,
1020 Peura, S., Vincent, W. F.: Increasing dominance of terrigenous organic matter in
1021 circumpolar freshwaters due to permafrost thaw, *Limnol. Oceanogr. Lett.*, 3, 2018, 186–
1022 198, 2012.

1023 Weishaar, J. L., Aiken, G. R., Bergamaschi, B. A., Fram, M. S., Fujii, R., and Mopper, K.:
1024 Evaluation of specific ultraviolet absorbance as an indicator of the chemical composition
1025 and reactivity of dissolved organic carbon, *Environ. Sci. Technol.*, 37, 4702–4708, 2003.

1026 Wickland, K. P., Aiken G. R., Butler K., Dornblaser M. M., Spencer R. G. M., and Striegl R.
1027 G.: Biodegradability of dissolved organic carbon in the Yukon River and its tributaries:
1028 seasonality and importance of inorganic nitrogen. *Glob Biogeochem Cycle* 26,
1029 2012gb004342, 2012.

1030 Wilske, C., Herzsprung, P., Lechtenfeld, O.J., Kamjunke, N., and von Tümpling, W.:
1031 Photochemically induced changes of dissolved organic matter in a humic-rich and forested
1032 stream, *Water*, 12, 331. <https://doi.org/10.3390/w12020331>, 2020.

1033 Winter, A. R., Fish, T. A. E., Playle, R. C., Smith, D. S., and Curtis, P. J.: Photodegradation of
1034 natural organic matter from diverse freshwater sources, *Aquat. Toxicol.*, 84, 215–222,
1035 2007.

1036 Zabelina, S.A., Shirokova, L.S., Klimov, S.I., Chupakov, A.V., Lim, A.G., Polishchuk, Y.M.,
1037 Polishchuk, V.Y., Bogdanov, A.N., Muratov, I.N., Guerin, F., Karlsson, J., and Pokrovsky,
1038 O.S.: Carbon emission from thermokarst lakes in NE European tundra, *Limnol. Oceanogr.*,
1039 66, S216–S230. <https://doi.org/10.1002/lno.11560>, 2021.

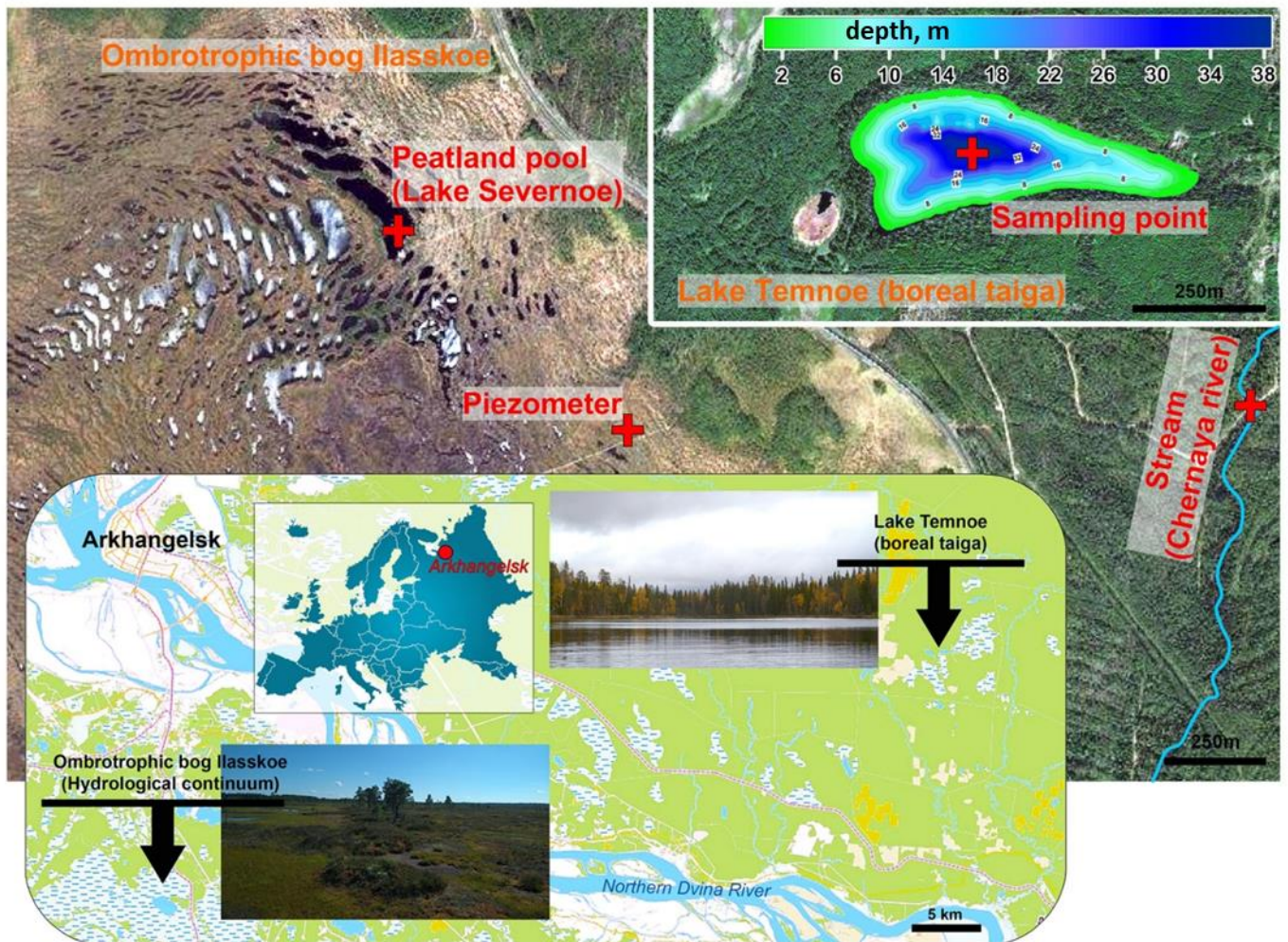
1041

1042

1043

1044

1045



1046

1047

1048 **Fig. 1.** Geographical location of studied hydrological continuum for Ilasskoe Bog waters and
1049 deep stratified Lake Temnoe in the boreal forest. Photo and map credits of Chupakov A.V.

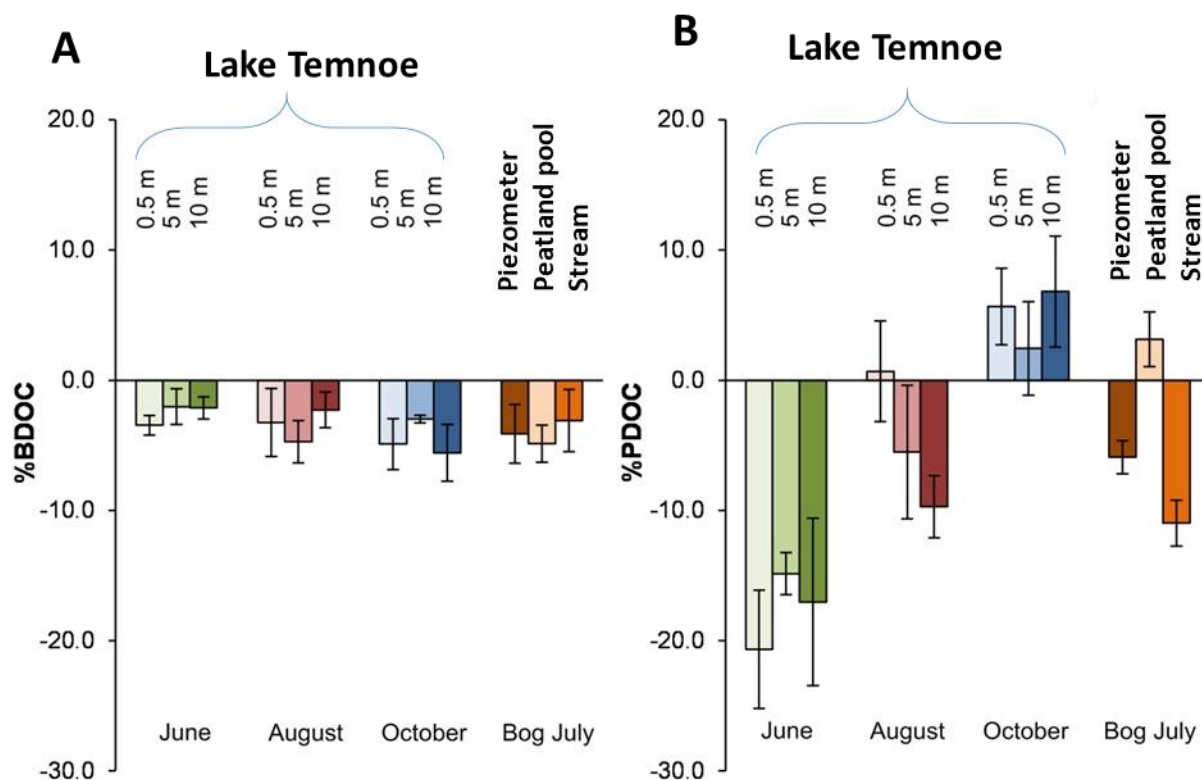
1050

1051

1052

1053

1054



1055

1056

1057

1058

1059 **Fig. 2.** Percentage of bio- (A) and photo- (B) degradable DOC presented as relative decrease in
1060 DOC concentration between the initial and final value for the Temnoe Lake (June, August and
1061 October) and Ilasskoe Bog surface waters (July). Error bars are 1 s.d. of duplicates relative to
1062 the control (see Eqn. 1-2 in the text). In accord with unified protocol of biodegradation
1063 experiments (Vonk et al., 2015), positive values signify nil photodegradation (experimental
1064 artifacts of DOC production).

1065

1066

1067

1068

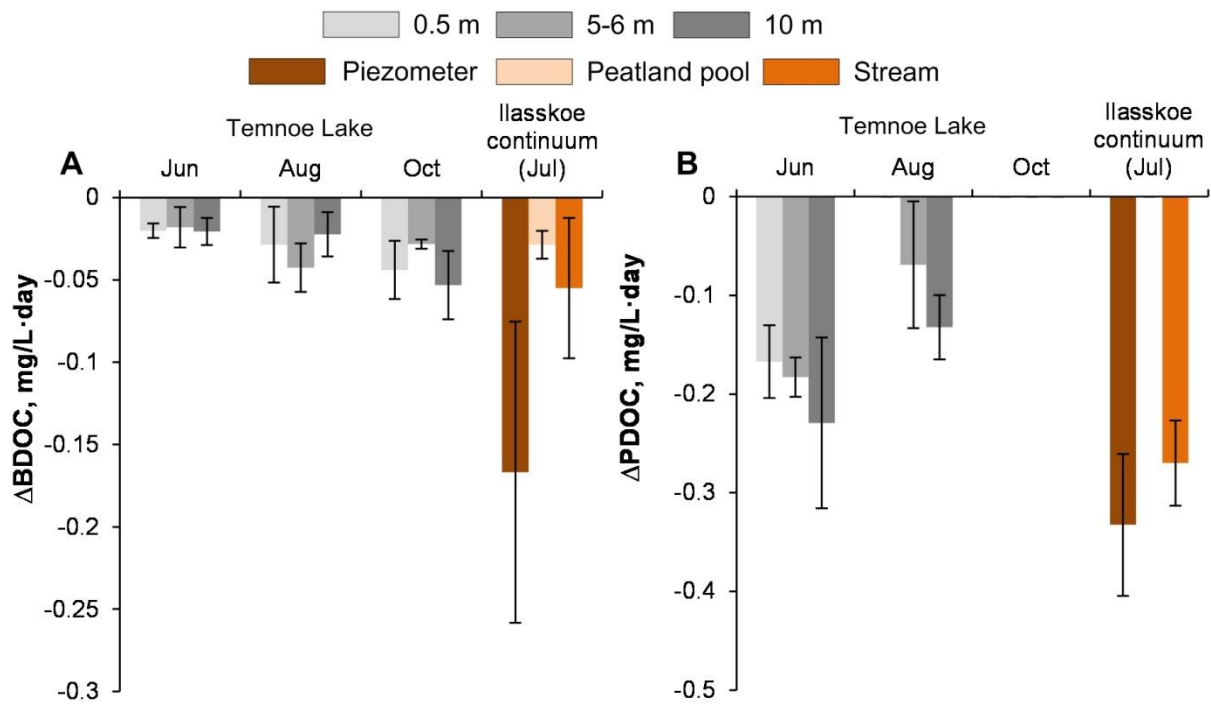
1069

1070

1071

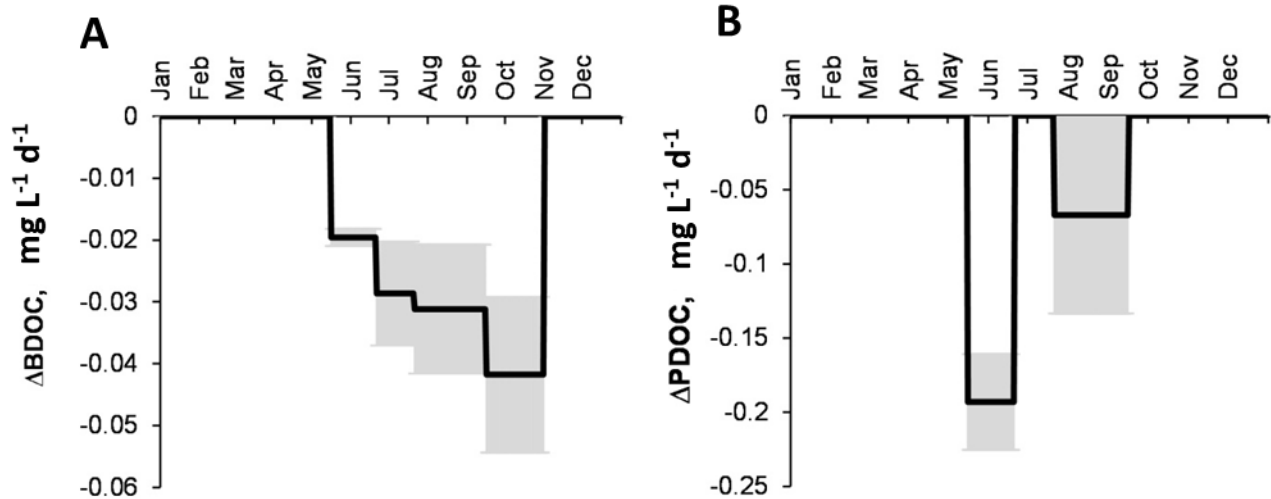
1072

1073
1074
1075
1076
1077
1078
1079



1080
1081
1082
1083
1084
1085
1086
1087
1088

Fig. 3. Rates of DOC bio- (A) and photo- (B) degradation. The values are negative because they represent a decrease in DOC concentration over the course of the experiment.



1089

1090

1091

1092 **Fig. 4.** Integral rates of bio- (ΔBDOC , **A**) and photo- (ΔPDOC , **B**) degradation in the 0-10 m
 1093 layer of Lake Temnoe across the entire open-water period (May to October). Rate values are
 1094 negative because they signify a decrease in DOC concentration. Note that there was no
 1095 sampling from December to April and the photodegradation was not studied in July.
 1096 Uncertainties are represented by gray shaded rectangles.

1097

1098

1099

1100

1101

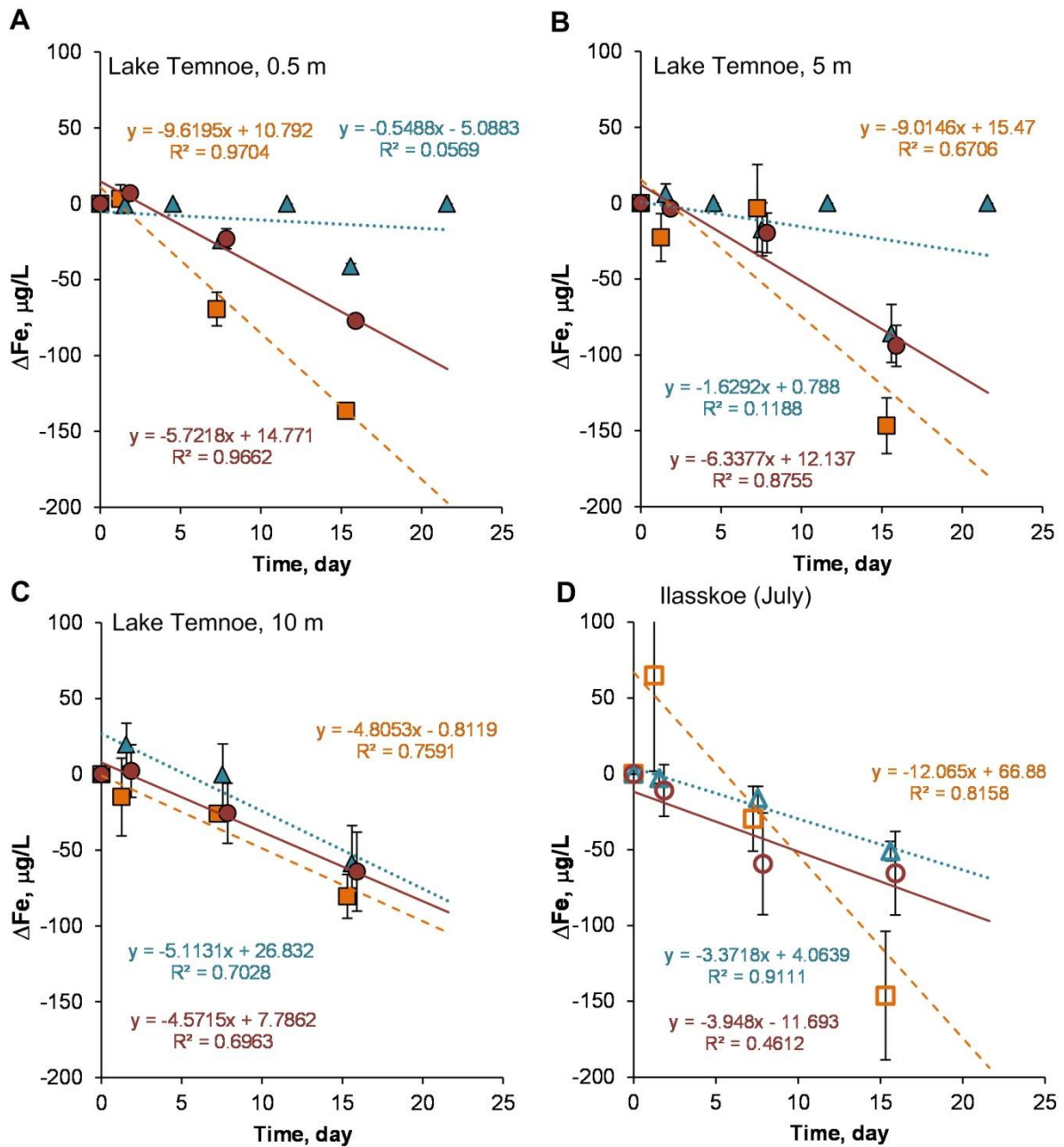
1102

1103

1104

1105

1106



1107

■ June ▲ August ● October □ Piezometer ▲ Peatland pool ○ Stream

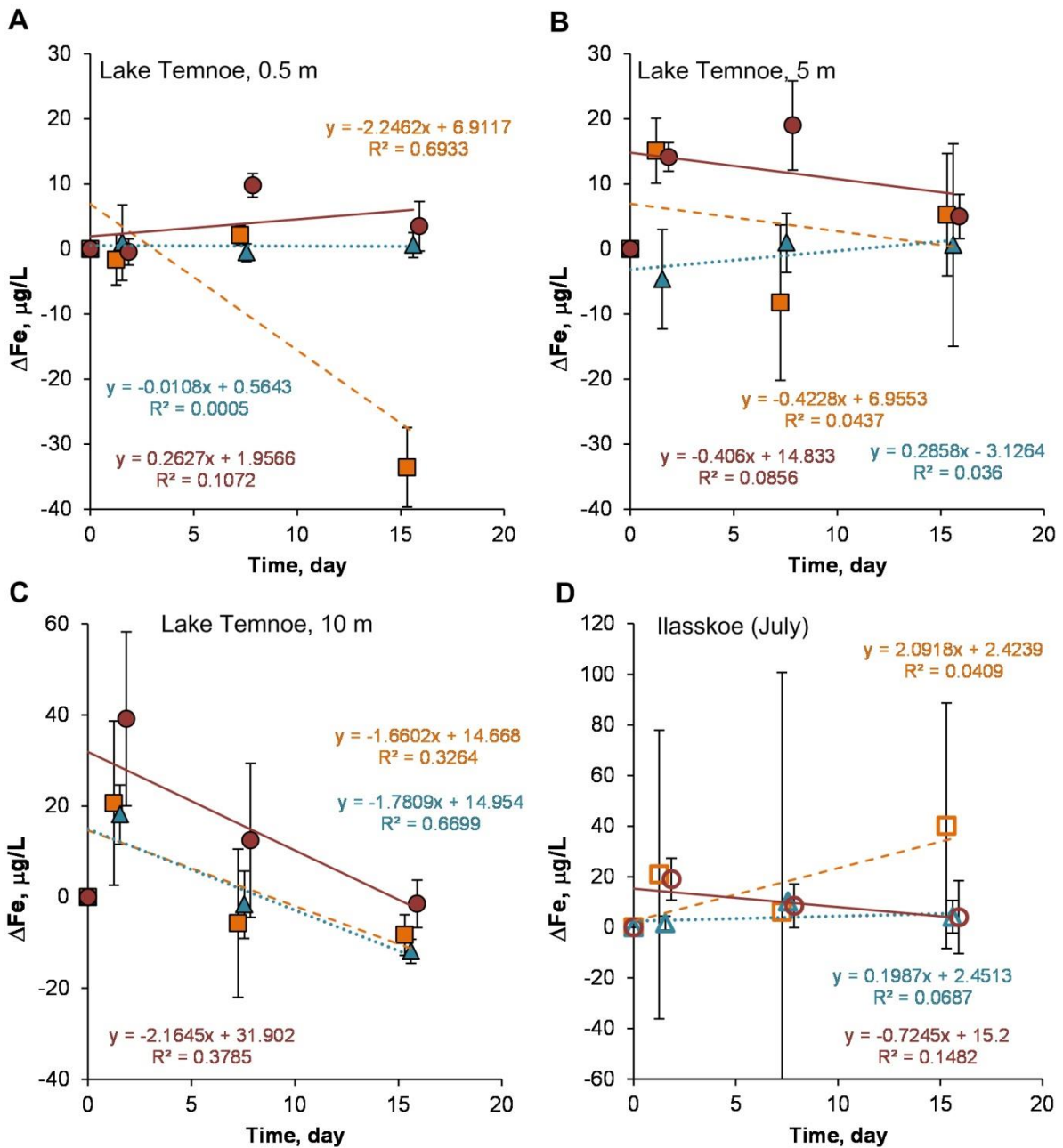
1108

1109 **Fig. 5.** Change in Fe concentration (relative to control) over time in biodegradation
 1110 experiments. Error bars are 1 s.d. of duplicates. Temnoe Lake 0.5 m (A), 5 m (B) and 10 m (C)
 1111 in June (squares), August (triangles) and October (circles). Ilasskoe Bog continuum in July (D)
 1112 including piezometer (squares), Severnoe peatland pool (triangles) and stream Chernyi
 1113 (circles).

1114

1115

1116



■ June
 ▲ August
 ● October
 Piezometer
 Peatland pool
 Stream

1117
 1118
 1119
 1120
 1121
 1122
 1123
 1124
 1125
 1126
 1127
 1128

Fig. 6. Change in Fe concentration (relative to the control) over time in photo-degradation experiments. The error bars are 1 s.d. of duplicates. Lake Temnoe 0.5 m (A), 5 m (B) and 10 m (C) in June (squares), August (triangles) and October (circles). Ilasskoe continuum in July (D) includes piezometer (squares), peatland pool Severnoe (triangles) and stream Chernyi (circles)

1129 **Table 1.** Landscape setting, hydrochemical characteristics and CO₂ concentration and emission
 1130 flux of studied waters. S.C. is specific conductivity and EB and OB is eutrophic and
 1131 oligotrophic bacteria count, respectively.

1132 **1A.** Plasskoe bog continuum in July.

1133

	Piezometer	Lake Severnoe	Stream Chernyi
GPS coordinates	N64.328694° E40.612556°	N64.334361° E40.609667°	N64.330982° E40.653352°
Description	Shallow groundwater	Peatland pool	Outlet stream
T, °C	11.4	19.4	13
O₂, mg/L	0.6	8.6	7.5
pH	3.9	4.0	5.7
S.C., μS cm⁻¹	46	17	26
DOC, mg L⁻¹	87.6	12.7	38.4
DIC, mg L⁻¹	0.32	0.40	0.38
SUVA₂₅₄	4.13	3.80	4.85
P-PO₄, μg L⁻¹	8.6	3.0	1.7
P_{total}, μg L⁻¹	153	10	20
N-NO₃, μg L⁻¹	111	70	98
N-NH₄, μg L⁻¹	85.4	16.1	12.6
N_{total}, μg L⁻¹	1180	222	399
Si, μg L⁻¹	1808	47	2076
CO₂, μmol/L	3360	55	318
CO₂ flux, mmol m⁻² d⁻¹	1600	22	151
EB, CFU mL⁻¹	49360	56600	9000
OB, CFU mL⁻¹	54560	37900	21600

1134

1135 **1B.** Lake Temnoe across seasons and depths.

1136

1137

Month	Jun	Jun	Jun	Aug	Aug	Aug	Oct	Oct	Oct
	0.5	5	10	0.5	5	10	0.5	6	10
GPS	N64.47683° E041.74533°								
Description	Lake in the northern taiga								
T, °C	12.7	4,9	4,5	18.4	5.5	4.3	9.0	5.8	4.4
O₂, mg/L	8,45	4,8	4,5	7.78	4.93	2.63	8.90	4.46	2.14
pH	5.2	5.2	5.3	6.0	5.5	5.7	5.2	5.2	5.1
S.C., μS cm⁻¹	17	17	19	17	17	19	18	18	20
DOC, mg L⁻¹	12.6	19.2	21	19	19.5	21.2	19.4	20.6	20.6
DIC, mg L⁻¹	0.55	0.53	0.49	0.70	0.71	0.66	0.67	0.67	0.64
SUVA₂₅₄	4.6	4.7	4.6	4.2	4.5	4.5	4.3	4.3	4.7
P-PO₄, μg L⁻¹	2.9	3.3	6.4	0.9	3.6	9.4	3.8	4.6	4.2
P_{total}, μg L⁻¹	19	17	19	20	16	20	18	19	20
N-NO₃, μg L⁻¹	119	150	137	86	152	254	88	85	100
N-NH₄, μg L⁻¹	7.1	8.0	10.0	9.1	17.5	13.8	16.4	14.1	15.5
N_{total}, μg L⁻¹	305	420	408	355	315	337	425	416	396
Si, μg L⁻¹	1940	2268	2354	1183	2208	2714	2269	2380	2380
CO₂, μmol/L	99	309	329	110	256	337	223	232	253
CO₂ flux, mmol m⁻² d⁻¹	32	-	-	46	-	-	71	-	-
EB, CFU mL⁻¹	-	36	50	259	92	270	780	220	105
OB, CFU mL⁻¹	50	570	420	-	190	-	680	150	66

1138

Table 2. The % bio- and photodegradable solutes (mean \pm s.d.) whose relative change (concentration decrease) in the course of experiment was superior to that of SD. Prefix ΔB and ΔP represents the effect of bio- and photodegradation, respectively. Duration of biodegradation and photodegradation is 21.6 ± 0.1 and 15.6 ± 0.1 days, respectively. W represents the probability of measurable effect, significantly different from changes in the control reactors. Only the components with $W \geq 33\%$ are presented. Temnoe Lake is deep stratified lake in the forest. Peizometer, peatland pool and outlet stream represent the hydrological continuum of the Ilasskoe Bog.

Index	Temnoe Lake		Temnoe Lake		Temnoe Lake		Temnoe Lake		Temnoe Lake		Temnoe Lake		Piezo-meter (Jul)		Peatland pool (Jul)		Outlet stream (Jul)	
	0.5 m (Jun)	5 m (Jun)	10 m (Jun)	0.5 m (Aug)	5 m (Aug)	10 m (Aug)	0.5 m (Oct)	5 m (Oct)	10 m (Oct)	0.5 m (Oct)	6 m (Oct)	10 m (Oct)	10 m (Oct)					
$\bar{\alpha}$, $\mu S/cm$	17	17	19	17	17	17	18	18	19	18	18	18	20	46	17	26		
$\Delta B(\bar{\alpha} \pm SD)$	-24 \pm 4	-26 \pm 7	-30 \pm 5	-23 \pm 3	-27 \pm 3	-27 \pm 3	-24 \pm 7	-23 \pm 4	-33 \pm 16	-24 \pm 7	-23 \pm 4	-17 \pm 5		0	-18 \pm 10	-29 \pm 4		
DOC, mg/L	12.6	19.2	21.0	19.0	19.5	19.5	19.4	20.6	21.2	19.4	20.6	20.6		87.6	12.7	38.4		
$\Delta B(DOC \pm SD)$	3.4 \pm 0.8	2.0 \pm 1.4	2.1 \pm 0.8	3.2 \pm 2.6	4.7 \pm 1.6	4.7 \pm 1.6	4.9 \pm 2.0	3.0 \pm 0.3	2.3 \pm 1.4	4.9 \pm 2.0	3.0 \pm 0.3	5.6 \pm 2.2		4.1 \pm 2.3	4.9 \pm 1.4	3.1 \pm 2.4		
$\Delta P(DOC \pm SD)$	20.7 \pm 4.6	14.9 \pm 1.6	17.0 \pm 6.4	0	5.5 \pm 5.1	0	9.7 \pm 2.4	0	9.7 \pm 2.4	0	0	0		5.9 \pm 1.3	0	11.0 \pm 1.8		
Al, $\mu g/L$	275	298	329	254	296	296	275	288	335	275	288	323		276	59	388		
$\Delta B(Al \pm SD)$	3.5 \pm 1.4	1.8 \pm 0.9	0	2.0 \pm 1.3	0	1.4 \pm 1.5	2.0 \pm 1.9	0	1.4 \pm 1.5	2.0 \pm 1.9	0	0		0.9 \pm 2.2	0	1.3 \pm 1.8		
$\Delta P(Al \pm SD)$	1.9 \pm 1.1	2.7 \pm 0.9	3.6 \pm 1.3	0	2.5 \pm 1.3	0	1.7 \pm 2.0	0.7 \pm 0.9	1.7 \pm 2.0	0.7 \pm 0.9	0	0		0	0	0.8 \pm 0.9		
Ti, $\mu g/L$	1.5	2.1	2.6	1.1	2.0	2.0	1.7	1.9	2.6	1.7	1.9	2.5		3.7	0.6	5.0		
$\Delta B(Ti \pm SD)$	-9.2 \pm 1.6	-9.9 \pm 7.4	-2.6 \pm 2.7	-4.8 \pm 3.4	-1.8 \pm 2.7	0	-3.6 \pm 1.7	-1.0 \pm 3.1	0	-3.6 \pm 1.7	-1.0 \pm 3.1	-1.0 \pm 3.9		-2.3 \pm 3.6	-2.2 \pm 1.7	-1.4 \pm 2.2		
$\Delta P(Ti \pm SD)$	-0.1 \pm 3	-3 \pm 3	-8 \pm 3	0 \pm 0	-9 \pm 1	-3 \pm 2	-2 \pm 4	0	-3 \pm 2	-2 \pm 4	0	0		0	-20 \pm 4	-3.3 \pm 0.5		
V, $\mu g/L$	0.5	0.6	0.7	0.4	0.5	0.5	0.4	0.5	0.7	0.4	0.5	0.7		1.1	0.5	1.3		
$\Delta B(V \pm SD)$	-8.3 \pm 16.2	-5.4 \pm 3.2	-4.9 \pm 2.3	-6.8 \pm 7.5	-10.0 \pm 4.6	-1.7 \pm 1.6	-14.7 \pm 11	-13.9 \pm 4.3	-1.7 \pm 1.6	-14.7 \pm 11	-13.9 \pm 4.3	-16.1 \pm 1.7		-3.2 \pm 2.6	-0.2 \pm 3.4	-17.9 \pm 5.0		
Mn, $\mu g/L$	39	55	79	17	48	48	30	47	93	30	47	105		78	9	47		
$\Delta B(Mn \pm SD)$	0	0	-0.3 \pm 2.2	-31.8 \pm 1.3	-3.2 \pm 1.6	-0.6 \pm 2.2	-4.8 \pm 2.2	-3.2 \pm 1.7	-0.6 \pm 2.2	-4.8 \pm 2.2	-3.2 \pm 1.7	-0.4 \pm 0.1		0	0	-1.6 \pm 2.8		
Fe, $\mu g/L$	358	527	710	165	460	460	317	448	795	317	448	820		4402	157	1006		
$\Delta B(Fe \pm SD)$	-18.1 \pm 2.5	-9.1 \pm 2.6	-5.4 \pm 1.6	-13.5 \pm 1.0	-6.3 \pm 2.6	-1.4 \pm 1.9	-9.5 \pm 1.4	-7.8 \pm 1.9	-1.4 \pm 1.9	-9.5 \pm 1.4	-7.8 \pm 1.9	-3.3 \pm 1.8		-0.8 \pm 0.8	-13.6 \pm 4.3	-4.5 \pm 2.4		
$\Delta P(Fe \pm SD)$	-3.9 \pm 0.6	-2.0 \pm 1.9	-4.0 \pm 1.3	0	-2.9 \pm 1.5	-0.2 \pm 0.6	-1.2 \pm 0.4	0	-0.2 \pm 0.6	-1.2 \pm 0.4	0	0		0	0	0		

Index	Temnoe Lake 0.5 m (Jun)		Temnoe Lake 5 m (Jun)		Temnoe Lake 10 m (Jun)		Temnoe Lake 0.5 m (Aug)		Temnoe Lake 5 m (Aug)		Temnoe Lake 10 m (Aug)		Temnoe Lake 0.5 m (Oct)		Temnoe Lake 6 m (Oct)		Temnoe Lake 10 m (Oct)		Piezometer (Jul)	Peatland pool (Jul)	Outlet stream (Jul)	
Co, µg/L	0.28	0.39	0.68	0.07	0.30	0.65	0.18	0.31	0.74	0.45	0.06	0.30	0.45	0.06	0.30	0.45	0.06	0.30	0.45	0.06	0.30	0.30
ΔB(Co±SD)	-2.2±5.1	-1.2±2.1	-3.7±4.6	-32.7±2.6	-8.1±5.6	-2.7±3.3	-11.0±4.4	-9.1±5.1	-1.6±0.4	0	0	0	0	0	0	0	0	0	0	0	0	-20.6±27.8
Cu, µg/L	0.5	0.6	0.7	0.6	0.6	0.7	0.7	0.7	0.5	1.5	0.3	0.8	1.5	0.3	0.8	1.5	0.3	0.8	1.5	0.3	0.8	0.8
ΔB(Cu±SD)	0	0	0	-14.3±1.4	-6.8±4.0	-17.9±11.0	-5.3±4.8	-4.1±8.0	-1.4±12.3	0	0	0	0	0	0	0	0	0	0	0	0	-7.7±9.9
Ga, µg/L	0.017	0.022	0.026	0.012	0.016	0.023	0.017	0.015	0.024	0.126	0.016	0.066	0.126	0.016	0.066	0.126	0.016	0.066	0.126	0.016	0.066	0.066
ΔP(Ga±SD)	-14±6	-13±5	-10±4	0	-1±8	0	-10±4	0	0	-7±5	-5±8	-6±3	-7±5	-5±8	-6±3	-7±5	-5±8	-6±3	-7±5	-5±8	-6±3	-6±3
Y, µg/L	0.22	0.25	0.28	0.20	0.24	0.28	0.22	0.23	0.28	0.10	0.01	0.21	0.10	0.01	0.21	0.10	0.01	0.21	0.10	0.01	0.21	0.21
ΔP(Y±SD)	-1.3±4.6	-6.7±0.9	-5.3±2.5	0	-2.3±0.7	-1.0±1.6	-1.4±0.2	0	0	0	0	0	0	0	0	0	0	0	0	0	0	-5.8±2.7
Zr, µg/L	0.4	0.4	0.5	0.4	0.5	0.5	0.4	0.4	0.5	0.3	0.1	0.4	0.3	0.1	0.4	0.3	0.1	0.4	0.3	0.1	0.4	0.4
ΔP(Zr±SD)	-15±4	-14±0	-13±2	-9±20	-17±1	-14±3	-4±4	0	0	0	0	0	0	0	0	0	0	0	0	0	0	-32±3
Nb, µg/L	0.016	0.020	0.025	0.012	0.020	0.024	0.017	0.018	0.025	0.033	0.005	0.042	0.033	0.005	0.042	0.033	0.005	0.042	0.033	0.005	0.042	0.042
ΔB(Nb±SD)	-3.6±10.2	-1.7±7.0	0	-7.7±4.8	-1.1±2.6	0	-7.3±2.3	-1.5±6.3	-5.0±4.0	-2.4±1.5	0	0	-2.4±1.5	0	0	-2.4±1.5	0	0	-2.4±1.5	0	0	0
ΔP(Nb±SD)	-9±3	-8±3	-9±1	-6±23	-13±2	-10±5	-8±4	0	-3±3	0	0	0	0	0	0	0	0	0	0	0	0	-10±4
Ba, µg/L	4.8	5.1	5.8	4.6	5.0	5.7	4.9	4.8	5.6	54.4	1.5	56.8	54.4	1.5	56.8	54.4	1.5	56.8	54.4	1.5	56.8	56.8
ΔB(Ba±SD)	-2.2±0.7	-2.8±1.7	-1.0±2.7	0	0	0	-1.9±0.5	-1.7±3.7	-5.9±1.6	0	0	0	0	0	0	0	0	0	0	0	0	-1.3±3.4
La, µg/L	0.23	0.26	0.30	0.21	0.26	0.32	0.24	0.27	0.31	0.07	0.01	0.22	0.07	0.01	0.22	0.07	0.01	0.22	0.07	0.01	0.22	0.22
ΔB(La±SD)	-4.9±6.5	0	0	-3.9±0.9	-0.3±1.6	-2.6±1.5	-1.1±3.6	-2.4±1.2	-4.0±2.8	-0.8±10.4	-29.7±10.0	-2.0±2.8	-0.8±10.4	-29.7±10.0	-2.0±2.8	-0.8±10.4	-29.7±10.0	-2.0±2.8	-0.8±10.4	-29.7±10.0	-2.0±2.8	-2.0±2.8
ΔP(La±SD)	-3.8±3.6	-1.2±5.9	-2.0±2.7	0	-3.6±1.0	-3.2±1.6	-1.8±0.9	-2.6±1.0	0	0	0	0	0	0	0	0	0	0	0	0	0	0
Ce, µg/L	0.58	0.65	0.71	0.50	0.62	0.78	0.59	0.63	0.78	0.21	0.03	0.56	0.21	0.03	0.56	0.21	0.03	0.56	0.21	0.03	0.56	0.56
ΔB(Ce±SD)	-5.2±4.2	0	0	-4.4±0.7	-0.1±1.4	-0.8±1.0	-0.9±2.9	-0.8±1.1	-2.2±2.2	0	0	0	0	0	0	0	0	0	0	0	0	-9.3±5.9
ΔP(Ce±SD)	-4.9±1.9	-6.2±1.2	-1.1±1.7	0	-1.5±0.5	-3.2±1.7	-1.9±1.2	0	-0.047±0.46	-3.7±1.5	-2.4±1.6	-3.6±1.1	-3.7±1.5	-2.4±1.6	-3.6±1.1	-3.7±1.5	-2.4±1.6	-3.6±1.1	-3.7±1.5	-2.4±1.6	-3.6±1.1	-3.6±1.1

1141
1142
1143

Table 2, continued.

Index	Temnoe Lake 0.5 m (Jun)		Temnoe Lake 5 m (Jun)		Temnoe Lake 10 m (Jun)		Temnoe Lake 0.5 m (Aug)		Temnoe Lake 5 m (Aug)		Temnoe Lake 10 m (Aug)		Temnoe Lake 0.5 m (Oct)		Temnoe Lake 6 m (Oct)		Temnoe Lake 10 m (Oct)		Piezometer (Jul)	Peatland pool (Jul)	Outlet stream (Jul)
	0.075	0.085	0.094	0.069	0.082	0.105	0.077	0.084	0.102	0.027	0.005	0.070	0.027	0.005	0.070	0.027	0.005	0.070	0.027	0.005	0.070
Pr, µg/L	0.075	0.085	0.094	0.069	0.082	0.105	0.077	0.084	0.102	0.027	0.005	0.070	0.027	0.005	0.070	0.027	0.005	0.070	0.027	0.005	0.070
ΔB(Pr±SD)	-1.9±5.2	0	-4.0±1.1	0	-0.7±1.3	0	-0.9±1.6	0	-3.2±2.3	-3.0±1.7	-10.8±8.4	-1.7±2.3	-3.0±1.7	-10.8±8.4	-1.7±2.3	-3.0±1.7	-10.8±8.4	-1.7±2.3	-3.0±1.7	-10.8±8.4	-1.7±2.3
ΔP(Pr±SD)	-3.0±3.9	-5.5±0.9	-0.4±2.9	13.7±20.8	0	-6.1±2.8	0	-1.3±1.8	0	-0.01±2.4	-16.9±3.0	-2.4±2.1	-0.01±2.4	-16.9±3.0	-2.4±2.1	-0.01±2.4	-16.9±3.0	-2.4±2.1	-0.01±2.4	-16.9±3.0	-2.4±2.1
Nd, µg/L	0.33	0.34	0.39	0.29	0.33	0.42	0.33	0.32	0.41	0.11	0.02	0.27	0.11	0.02	0.27	0.11	0.02	0.27	0.11	0.02	0.27
ΔP(Nd±SD)	-7.8±2.4	-4.5±2.5	-0.8±2.1	0	-3.8±2.5	-2.0±3.3	0	-0.9±1.6	0	-3.8±2.5	-2.0±3.3	0	-0.9±1.6	0	-3.8±2.5	-2.0±3.3	0	-0.9±1.6	0	-3.8±2.5	-2.0±3.3
Eu, µg/L	0.015	0.017	0.016	0.012	0.016	0.020	0.014	0.018	0.021	0.011	0.001	0.017	0.011	0.001	0.017	0.011	0.001	0.017	0.011	0.001	0.017
ΔP(Eu±SD)	0	-10.9±3.3	0	0	-0.8±4.7	-3.0±4.0	0	-8.7±8.4	-6.9±4.2	-23.7±8.6	-58.2±15.2	-1.0±1.0	-23.7±8.6	-58.2±15.2	-1.0±1.0	-23.7±8.6	-58.2±15.2	-1.0±1.0	-23.7±8.6	-58.2±15.2	-1.0±1.0
Gd, µg/L	0.06	0.07	0.08	0.05	0.07	0.08	0.06	0.07	0.09	0.02	0.00	0.06	0.02	0.00	0.06	0.02	0.00	0.06	0.02	0.00	0.06
ΔP(Gd±SD)	-0.2±4.4	-6.5±2.9	-3.5±3.5	0	-6.0±3.2	-7.6±1.9	-2.3±2.0	0	-6.7±3.2	-6.0±3.2	-7.6±1.9	-2.3±2.0	0	-6.7±3.2	-6.0±3.2	-7.6±1.9	-2.3±2.0	0	-6.7±3.2	-6.0±3.2	-7.6±1.9
Ho, µg/L	0.009	0.009	0.011	0.007	0.009	0.011	0.009	0.009	0.011	0.004	0.0004	0.009	0.004	0.0004	0.009	0.004	0.0004	0.009	0.004	0.0004	0.009
ΔP(Ho±SD)	-1.9±1.5	-0.3±1.6	-4.6±6.5	0	-0.1±3.6	-3.4±3.2	-11.0±4.9	0	-21.5±11.3	-0.1±3.6	-3.4±3.2	-11.0±4.9	0	-21.5±11.3	-0.1±3.6	-3.4±3.2	-11.0±4.9	0	-21.5±11.3	-0.1±3.6	-3.4±3.2
Er, µg/L	0.023	0.025	0.033	0.022	0.026	0.030	0.022	0.023	0.031	0.011	0.001	0.023	0.011	0.001	0.023	0.011	0.001	0.023	0.011	0.001	0.023
ΔB(Er±SD)	0	0	0	-5.2±3.0	-2.1±1.8	0	-2.1±3.5	0	-2.0±5.3	-15.6±4.9	-22.9±19.5	0	-15.6±4.9	-22.9±19.5	0	-15.6±4.9	-22.9±19.5	0	-15.6±4.9	-22.9±19.5	0
Pb, µg/L	0.23	0.24	0.23	0.16	0.23	0.39	0.28	0.28	0.32	11	0.35	0.65	11	0.35	0.65	11	0.35	0.65	11	0.35	0.65
ΔB(Pb±SD)	0	0	0	-21.3±2.5	-2.0±7.6	-2.4±1.6	-8.2±3.3	-7.2±9.9	-0.8±2.7	0	-17.4±1.0	-8.5±10.9	0	-17.4±1.0	-8.5±10.9	0	-17.4±1.0	-8.5±10.9	0	-17.4±1.0	-8.5±10.9
Th, µg/L	0.046	0.052	0.066	0.058	0.054	0.064	0.053	0.054	0.061	0.019	0.005	0.050	0.019	0.005	0.050	0.019	0.005	0.050	0.019	0.005	0.050
ΔP(Th±SD)	0	0	-11.6±2.6	-12.2±22.5	-7.8±3.2	-18.1±5.6	0	-2.0±1.9	-2.0±1.9	-49.5±1.3	-10.6±0.8	-2.0±1.9	-49.5±1.3	-10.6±0.8	-2.0±1.9	-49.5±1.3	-10.6±0.8	-2.0±1.9	-49.5±1.3	-10.6±0.8	-2.0±1.9

1146
1147
1148
1149
1150

Table 3. Mean (\pm SD), depth-integrated rates of bio- and photodegradation ($\text{mg C L}^{-1}\text{d}^{-1}$)

Object	$V_{\text{Biodegradation}}$	$V_{\text{Photodegradation}}$
Lake Temnoe		
Forest Lake (Jun)	-0.02 ± 0.0014	-0.19 ± 0.03
Forest Lake (Aug)	-0.031 ± 0.010	-0.067 ± 0.066
Forest Lake (Oct)	-0.042 ± 0.013	0
Ilasskoe Bog continuum (July)		
Piezometer water	-0.17 ± 0.09	-0.33 ± 0.07
Peatland pool	-0.029 ± 0.008	0
Outlet stream (Chernyi)	-0.055 ± 0.043	-0.27 ± 0.043

1151
1152
1153
1154
1155
1156
1157
1158
1159